Study of the surface structure of materials using scanning probe microscopy (SPM).

- Arkadiusz Foks
- Supervisor: Dr hab. Dariusz Banaś, prof UJK
- 2nd Supervisor: Dr inż. Paweł Jagodziński
- Jan Kochanowski University

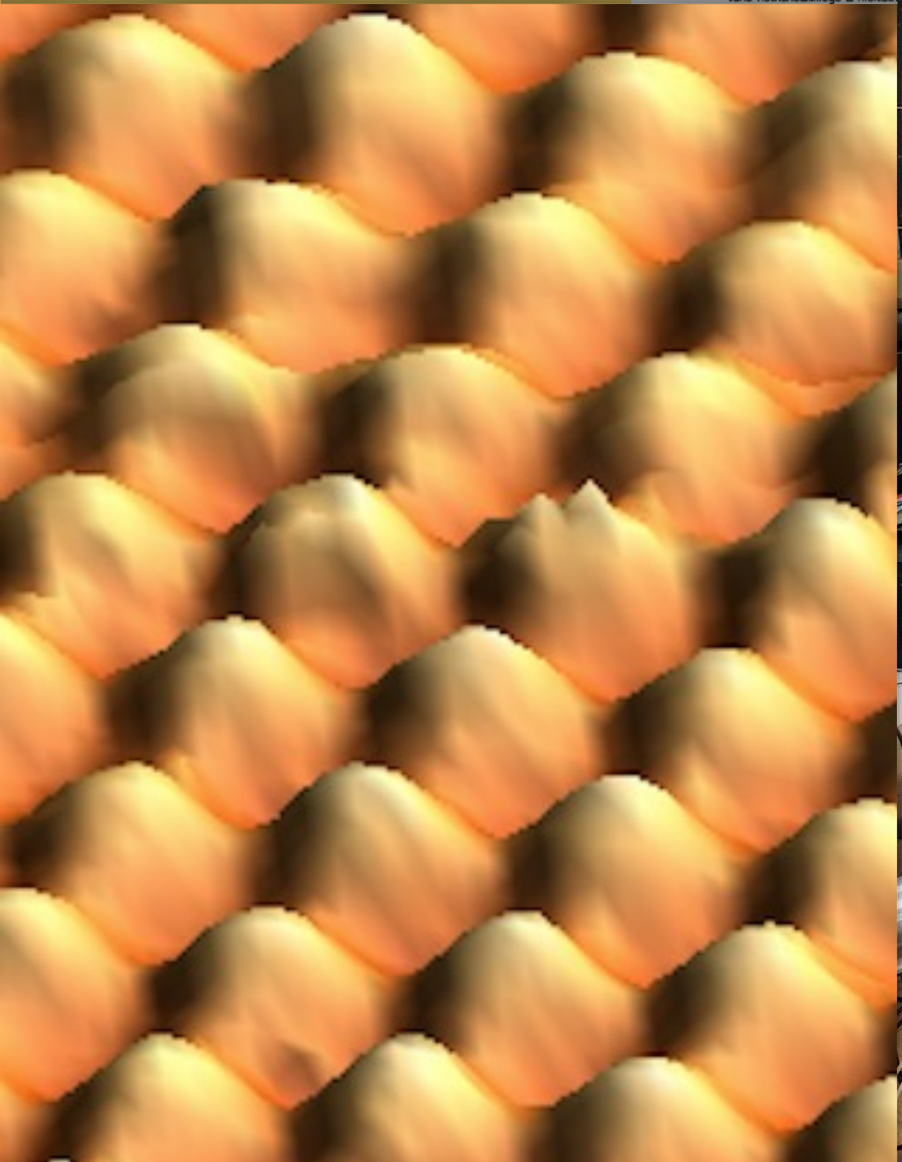

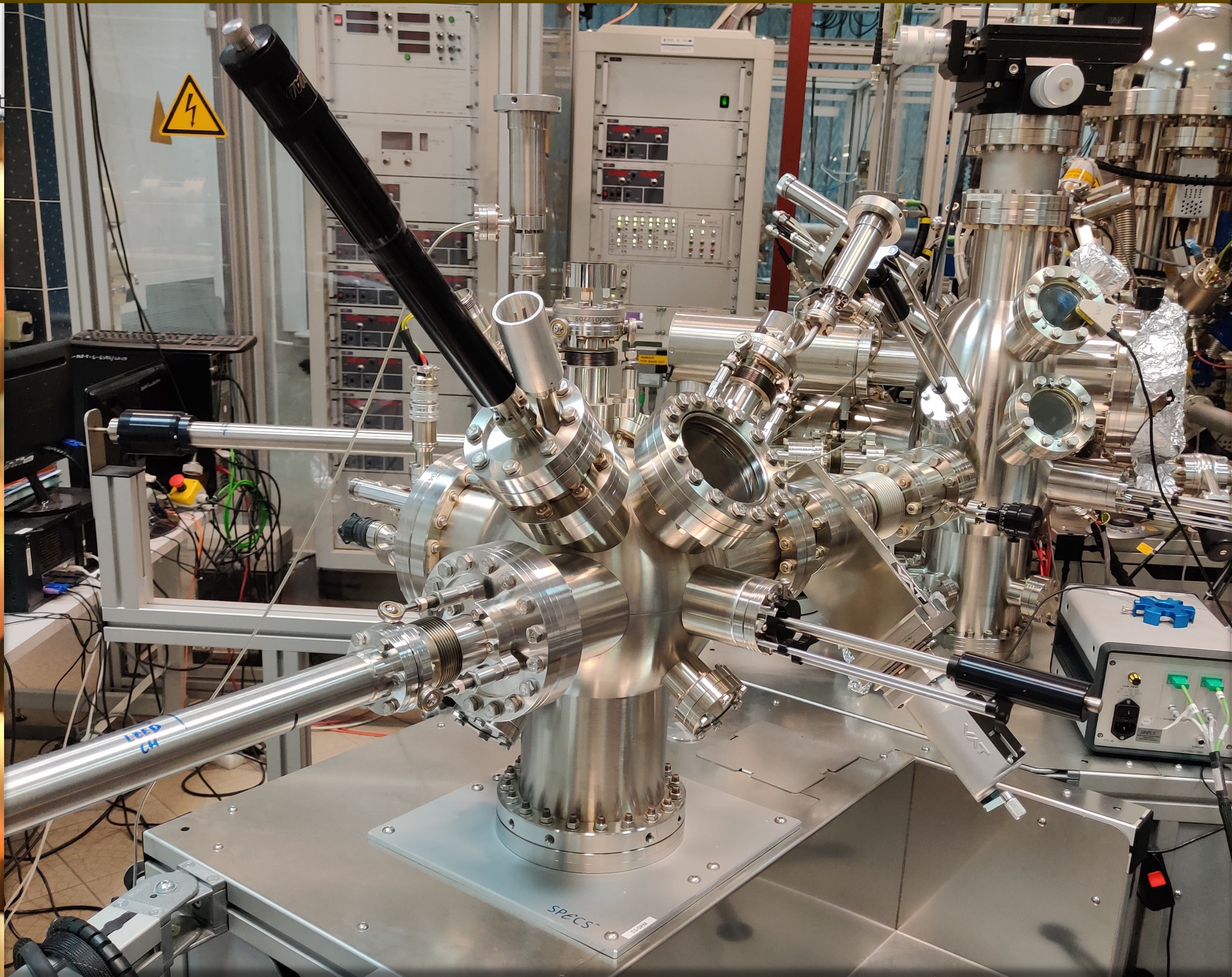

Outline

- Measured samples
- EBIS
- HCI irradiation
- Interaction effects of HCI with the surface
- Amorphous metals
- Measurements of formed nanostructures
- Thermal Spike Model
- Conclusions
- Plans for the near future

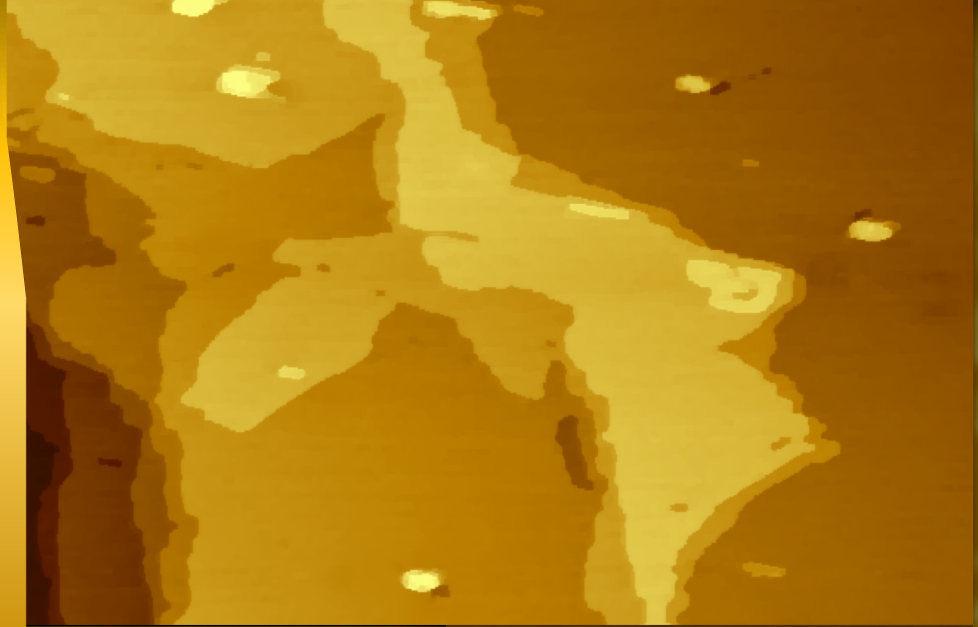

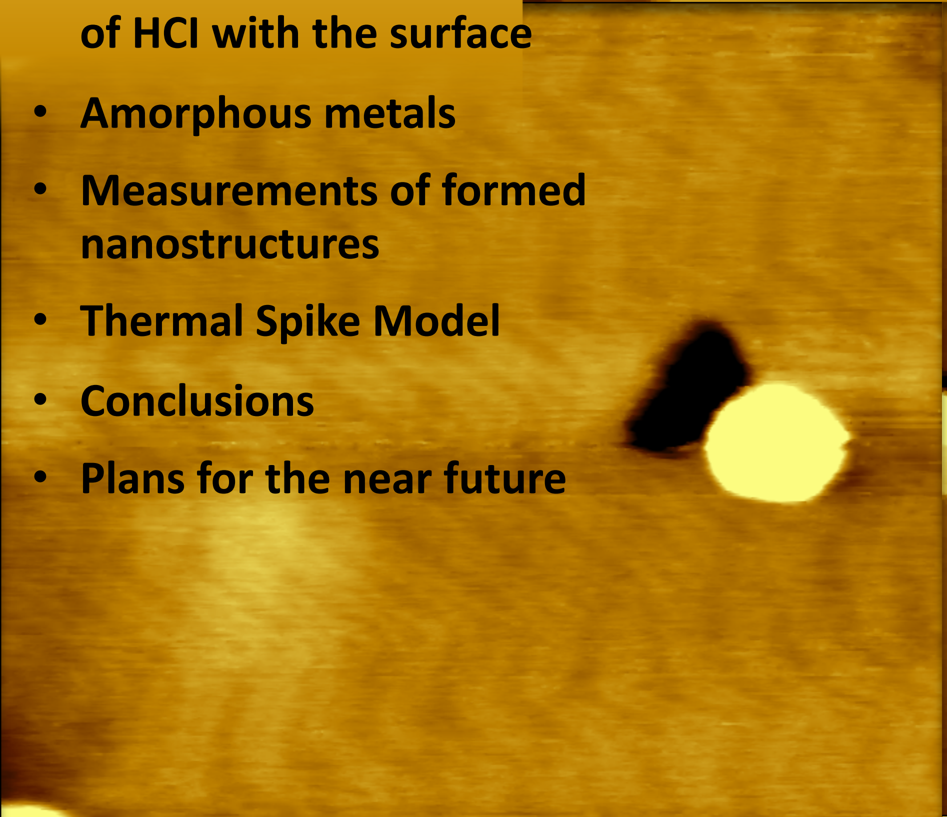

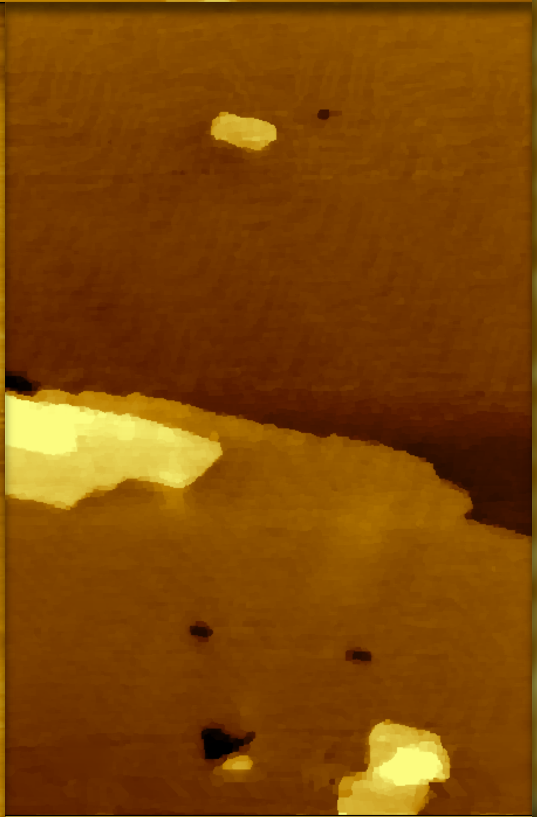

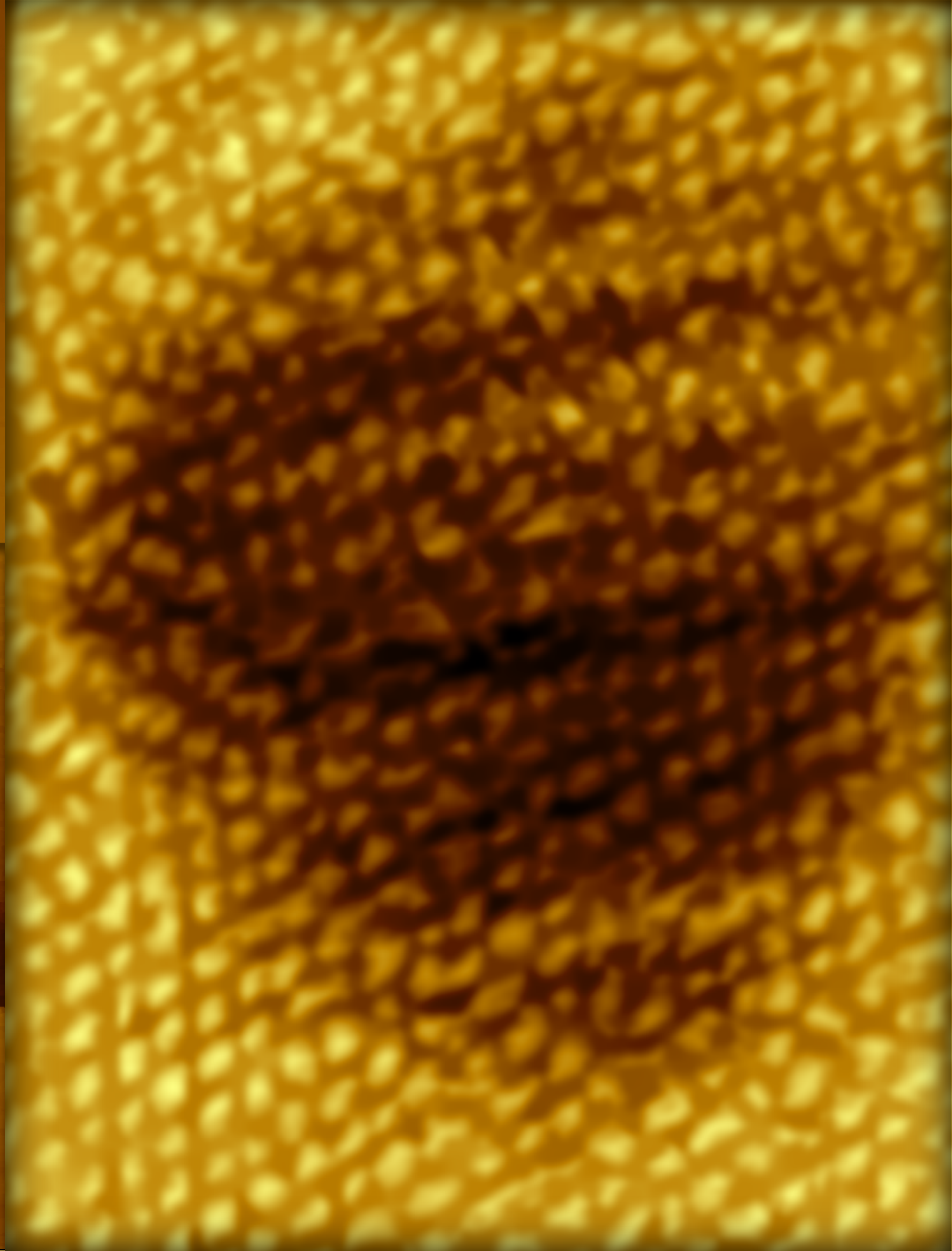

Quantum tunnelling

Quantum tunnelling is a phenomenon in which particles penetrate a potential energy barrier with a height greater than the total energy of the particles. The phenomenon is interesting and important because it violates the principles of classical mechanics.

The transmission through the barrier can be finite and depends exponentially on the barrier height and barrier width. The wavefunction may disappear on one side and reappear on the other side. The wavefunction and its first derivative are continuous. In steady-state the probability flux in the forward direction is spatially uniform. No particle or wave is lost. Tunnelling occurs with barriers of thickness around 1-3 nm and smaller.

Relation of the tunnelling current to the gap distance when the tunnelling gap is small and voltage is low can be simplified to:

$$I \propto \left(V/s\right)e^{-A\bar{\varphi}^{\frac{1}{2}}s}$$

Where A=1.025 $(\mathrm{eV})^{-1/2}$ Å^{-1}, φ is the average barrier height between the two electrodes, V is the bias potential between the sample and the tip, and s is the gap distance.

This equation indicates that a 1 Å change in the gap distance produces roughly one order of magnitude change of the tunnelling current with $\varphi \sim 4$ eV.

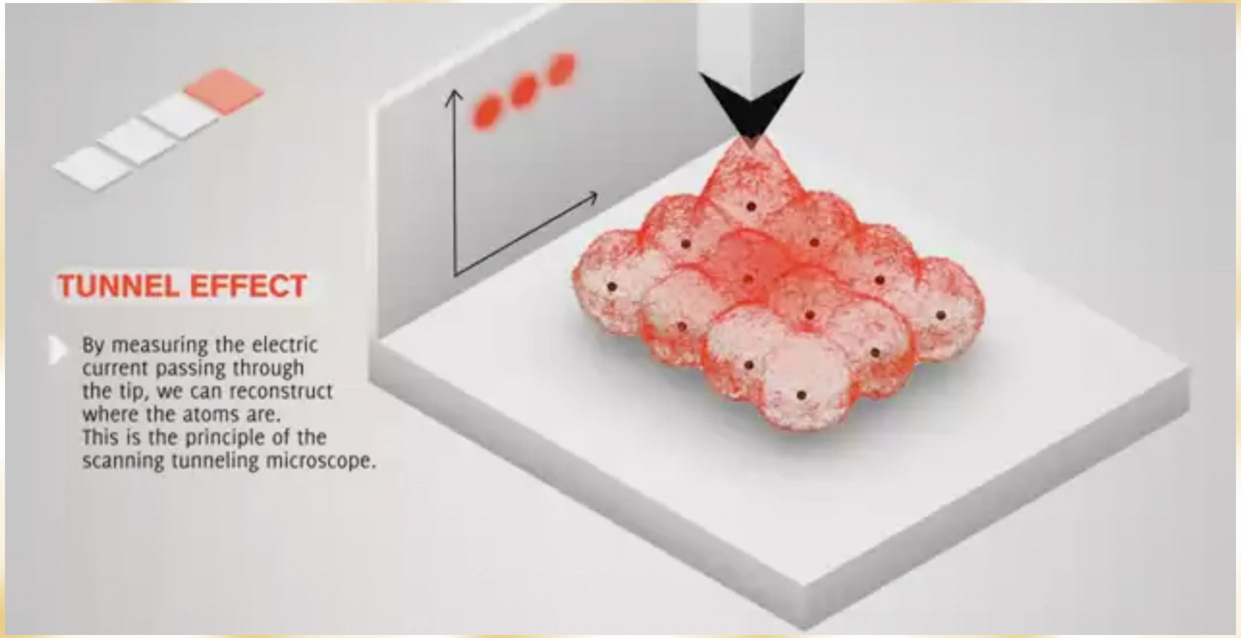

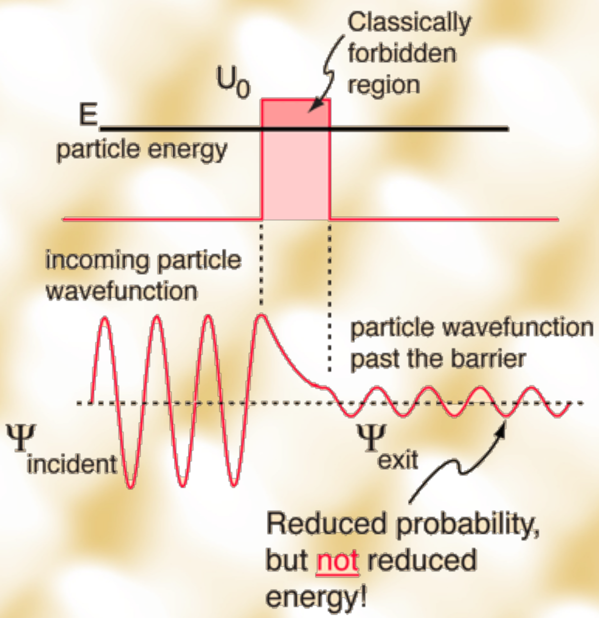

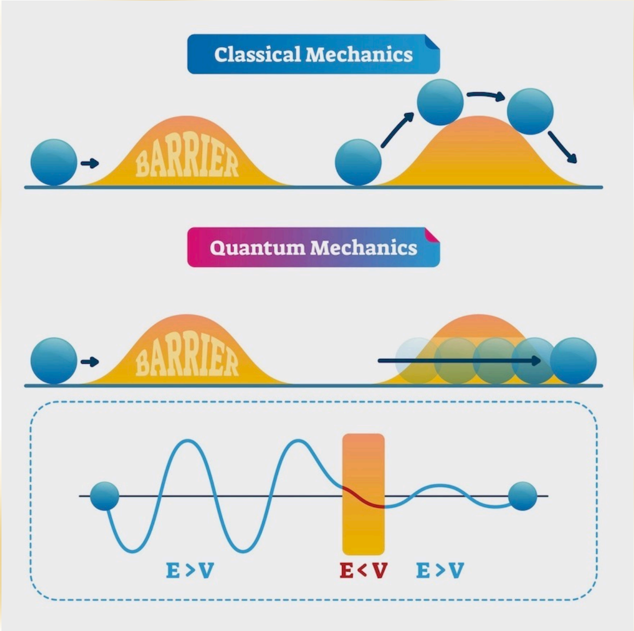

Graphene

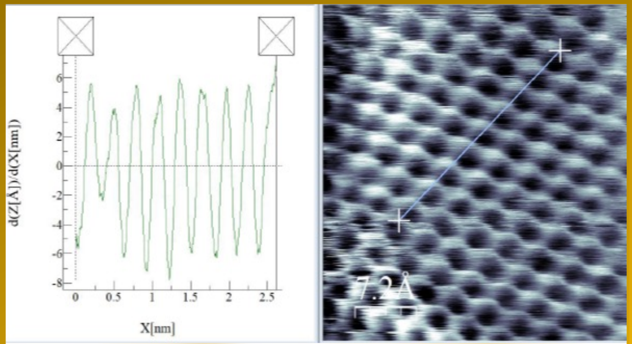

L.p.	Number of atoms	Total measured distance [nm]	Distance between unit cells [nm]
1	10	2.612	0.262
2	8	1.953	0.244
3	7	1.899	0.271
4	7	1.718	0.245
5	12	3.081	0.256
6	9	2.242	0.249
7	8	1.944	0.243
Average	-	-	0.253 ± 0.018

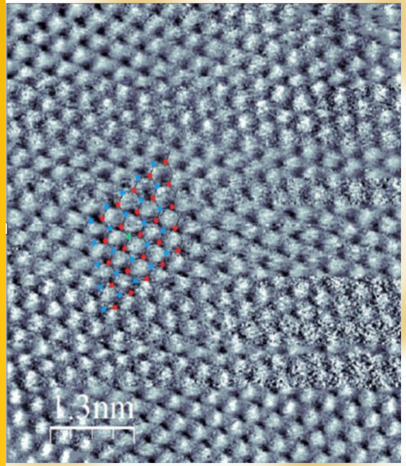

Theoretical value = 0.246nm Gray D. McCaughan A., Crystal Structure of Graphite, Graphene and Silicon

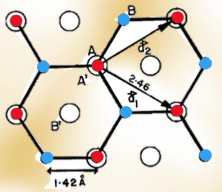

$$\frac{|0{,}246\ nm - 0{,}253\ nm|}{0{,}246\ nm} \cdot 100\ \% = 2{,}846\ \%$$

Au(111)

- Terrace profile
- Herringbone
- 23 x √3 cell reconstruction
- Atomic angles
- Atomic diameter
- Distance between nuclei
- Craters caused by ion irradiation
- Roughness

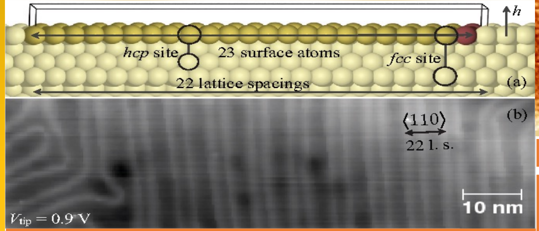

Measured distances in different structures show the existence of the 23 x √3 unit cell. In the distance of 22 atoms, the layer is compressed enough to fit one extra atoms i.e. 23 atoms in 22 lattice spacing.

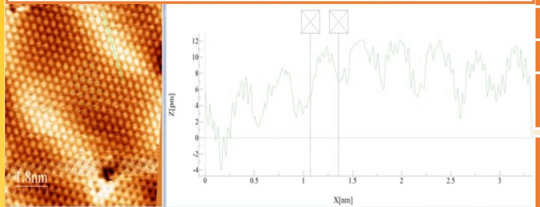

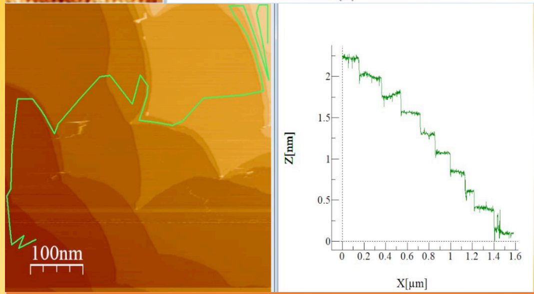

Distribution of ionization holes was done using Flooding function. Parameters were chosen basing on previous measurements. Function showed 571 holes covering 1.95% of scanned area.

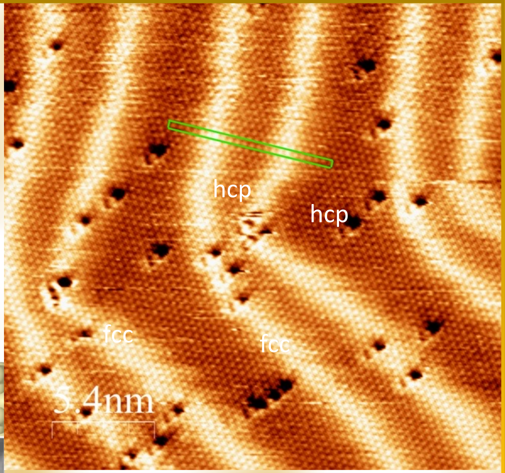

hcp		
No. of atoms	Row length	Distance between nuclei [nm]
4	1.310	0.328
6	1.958	0.326
5	1.569	0.314
5	1.626	0.325
6	1.983	0.331
Average	0.325 ± 0.011	

	Total height (nm)	Height difference (nm)
1	2.226	0.234
2	1.992	0.218
3	1.774	0.224
4	1.550	0.244
5	1.306	0.233
6	1.073	0.244
7	0.829	0.234
8	0.595	-
Interplanar distance		0.233 ± 0.015

Silicon substrate

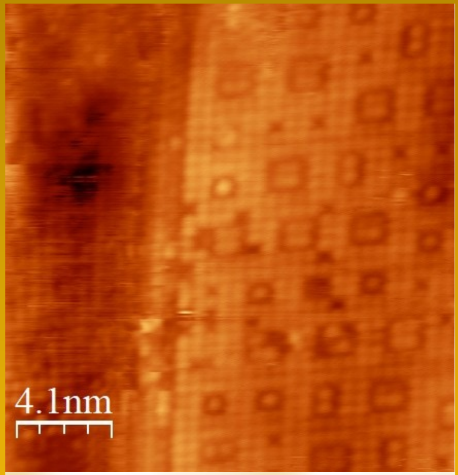

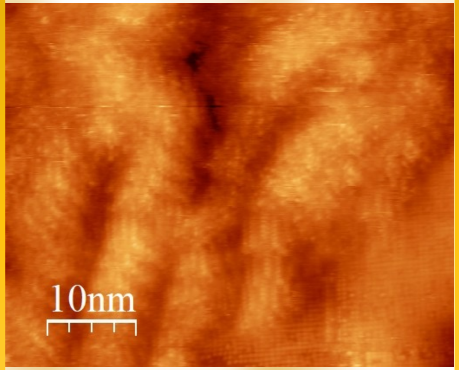

Images of the surface of Si(110) substrate in different scan areas.

Graph of the roughness (R.A) in the dependence of the scan area.

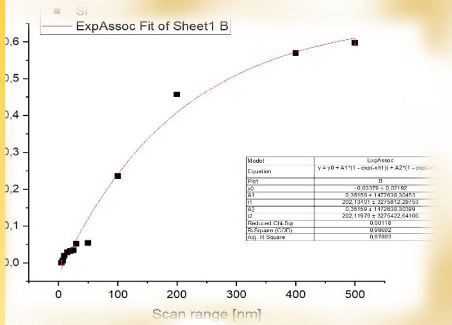

Cu(111)

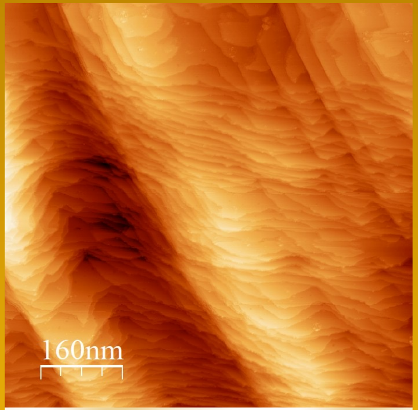

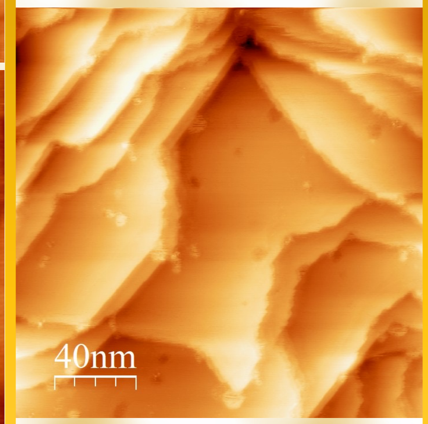

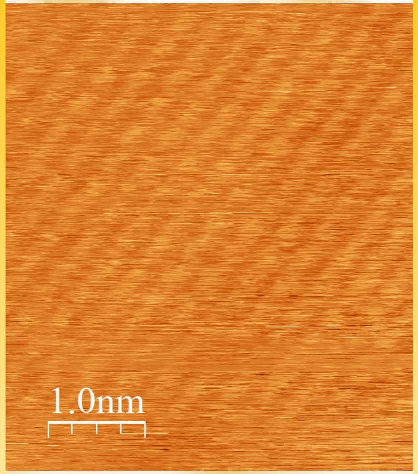

Nanolayers

Au/Si

Au 100 nm nanolayer

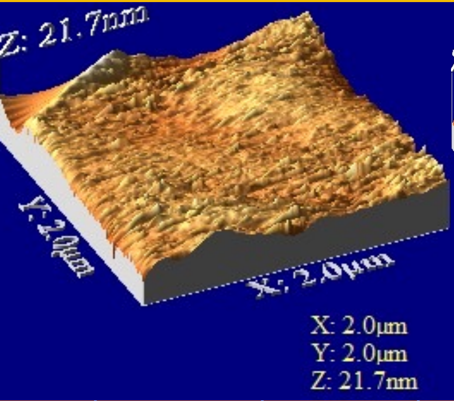

Au 25 nm nanolayer

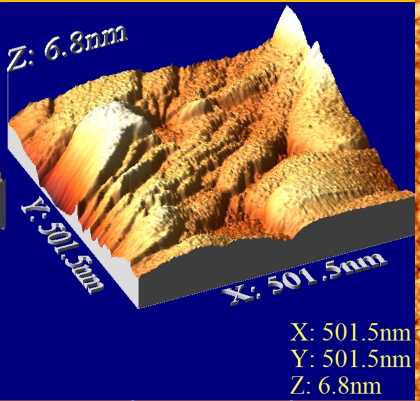

[nm]	2500 x 2500	2000 x 2000	1500 x 1500	1000 x 1000	500 x 500
Au (111)	-	-	-	-	0,112
Au (bulk)	-	-	-	-	0,474
Au 100	2,035	1,407	1,503	1,118	0,563
Au 25	2,897	2,741	2,31	1,569	0,789

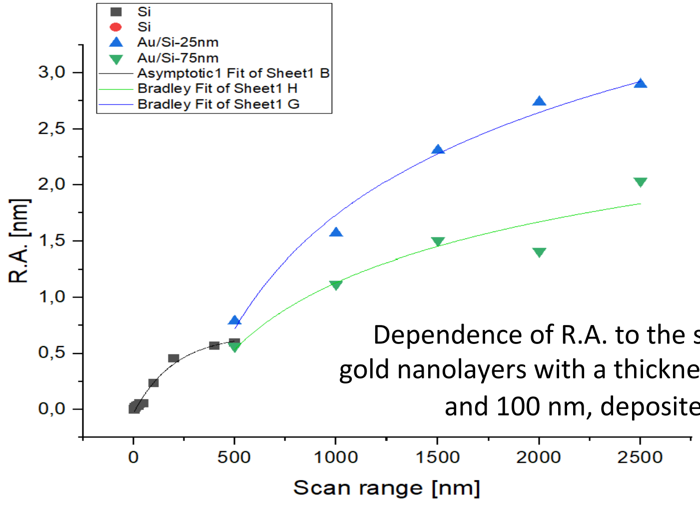

Dependence of R.A. to the scan area of gold nanolayers with a thickness of 25 nm and 100 nm, deposited on silicon substrate.

Ti/Si

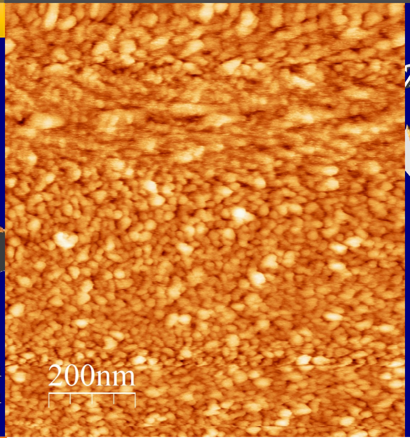

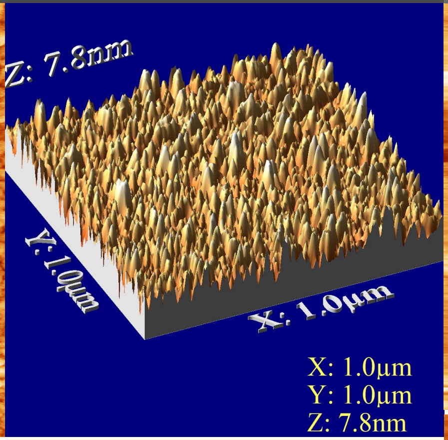

[nm]	Scan size	RMS	R.A.	Rskw	Rkur	IS
1	2500 x 2500	2,299	1,663	0,614	4,757	6,613
2	2000 x 2000	1,883	1,332	0,475	5,201	4,292
3	1500 x 1500	2,173	1,171	0,213	3,311	2,238
4	1000 x 1000	0,911	0,722	0,149	3,105	1,068
5	500 x 500	0,868	0,686	0,089	3,061	2,784

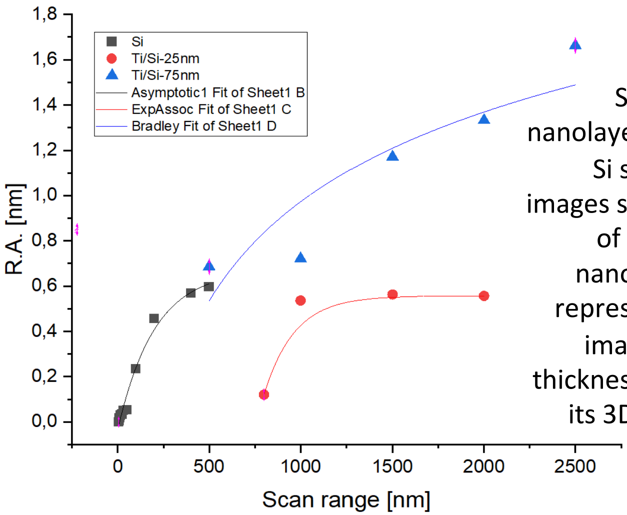

Scans of titanium nanolayers deposited on Si substrate. Upper images show the surface of 25 nm thickness nanolayer and its 3D representation. Lower representation. Lower images show 75 nm thickness nanolayer and its 3D representation

Ti/SiO_2

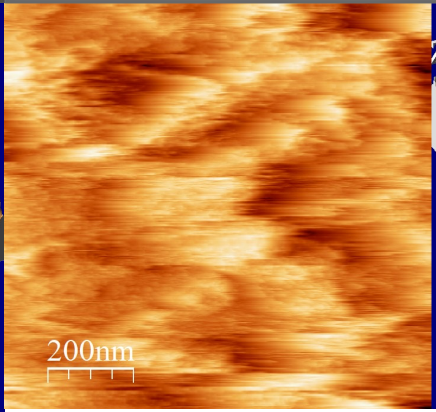

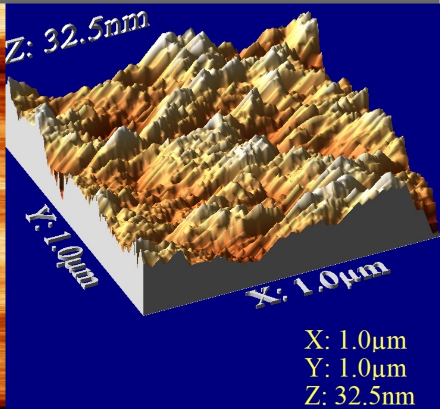

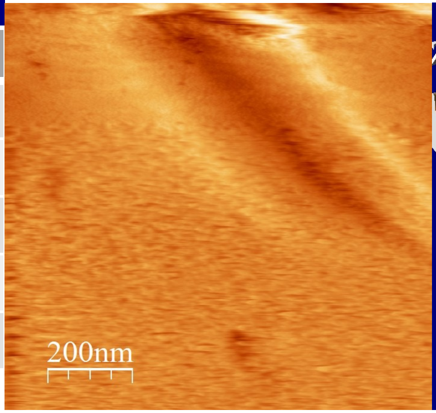

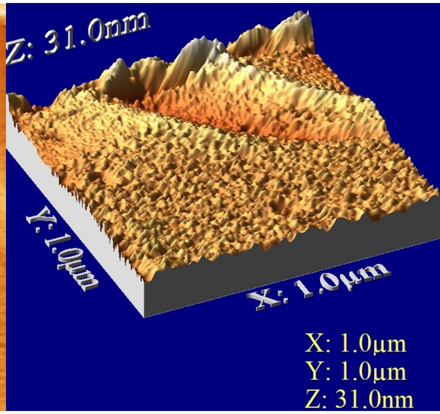

Scans of titanium nanolayers deposited on SiO_2 substrate, 25 nm and 75 nm thickness nanolayers and its 3D representation.

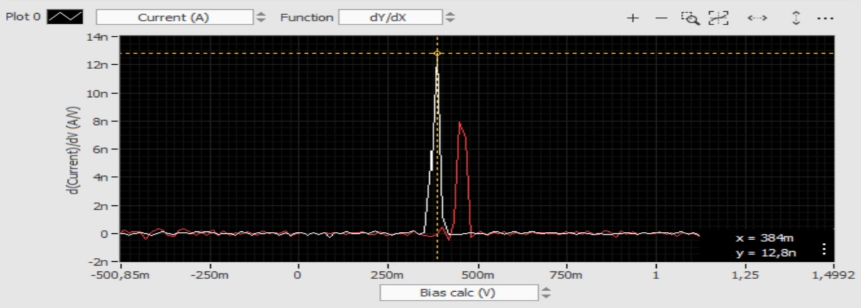

Scanning tunneling spectroscopy spectras of titanium nanolayers deposited on Si and SiO_2 substrate. Slight shift is visible.

Nanolayers roughness comparison

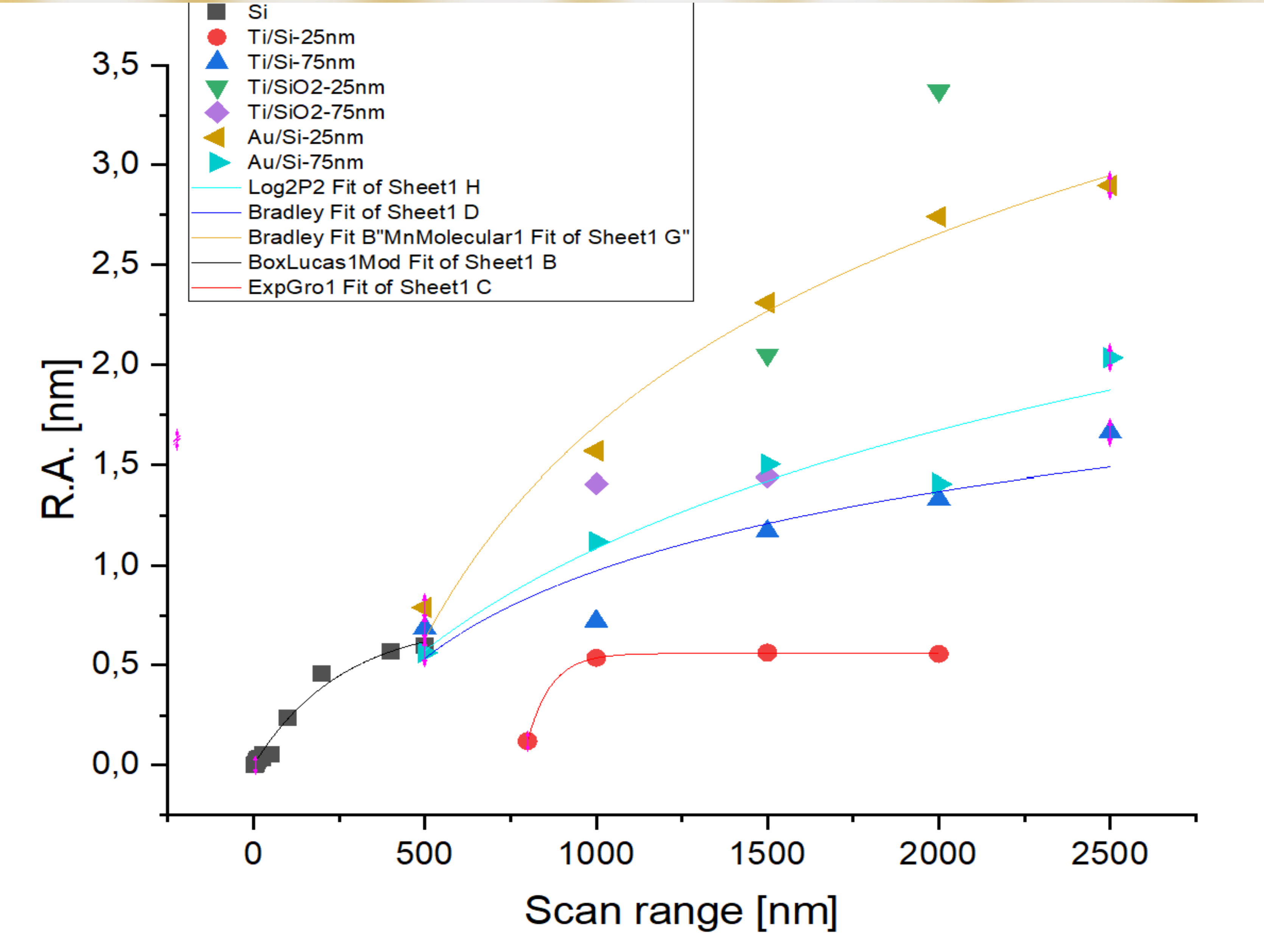

Hysteresis compensation

- Required to be proficient in Nanonis Software usage and data acquisition
- Surface with characteristic structures is needed to proceed
- Correction of the value of the voltage applied to the piezo to make scan linear in both scanning directions
- Set the compensation on both: fast and slow scan axis
- Possibility to set the know values of hysteresis compensation
- Real-time adjustment of voltage compensation values using Line Scan Monitor module

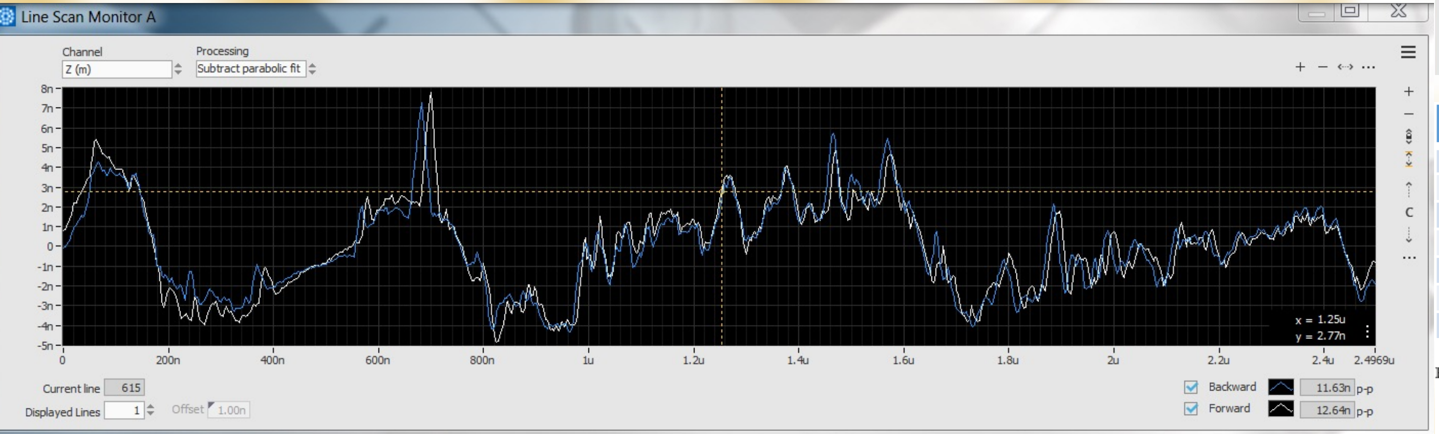

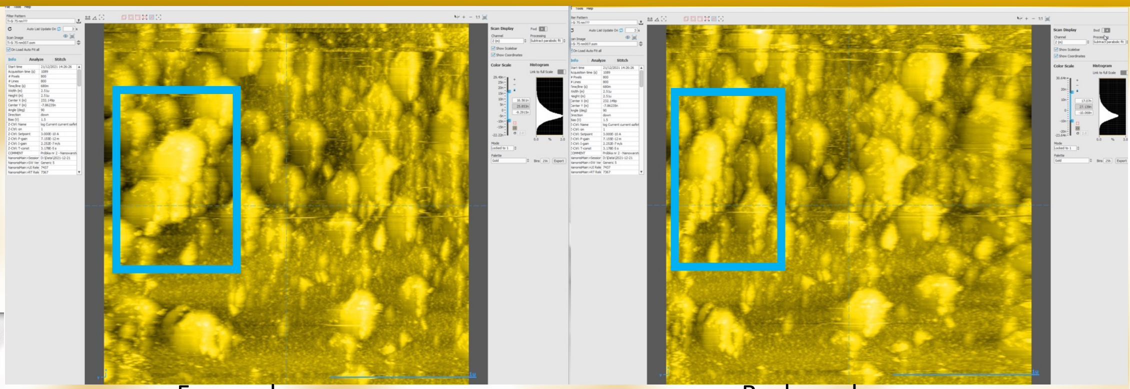

Forward scan	Backward scan	Dist. fwd to bwd	Compensation	Displacement fwd	Displacement bwd
0,033	1,132	1,128	0,227	0,095	0,194
0,336	0,573	0,237	0,564	-0,009	0,228
0,431	0,758	0,327	0,715	-0,043	0,284
0,900	1,279	0,379	1,222	-0,057	0,322
1,407	1,777	0,381	1,739	-0,038	0,332
1,947	2,208	0,237	2,222	0,014	0,275
2,269	2,388	0,119	2,562	0,174	0,293

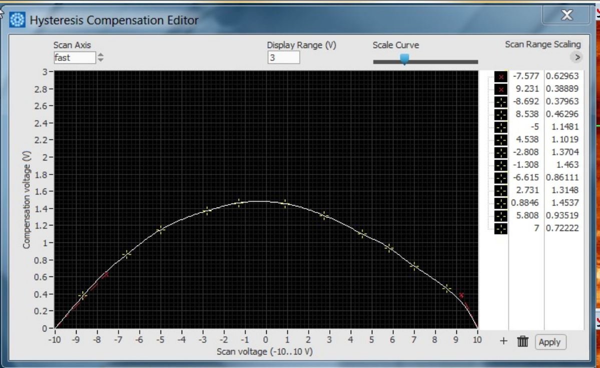

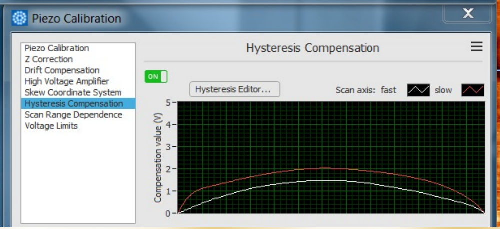

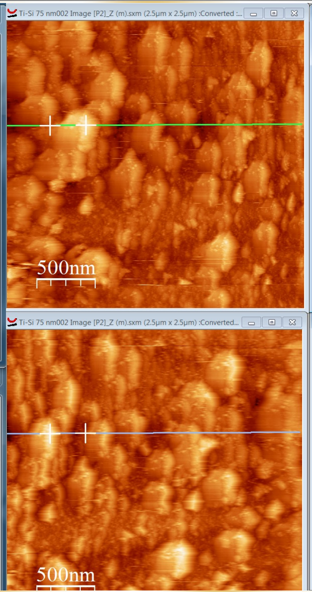

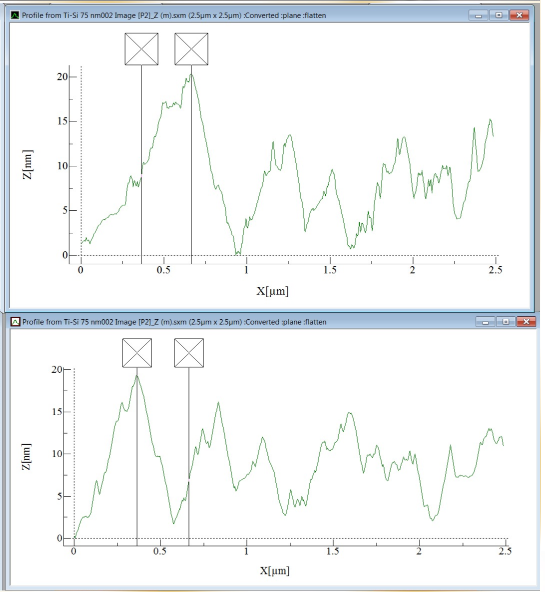

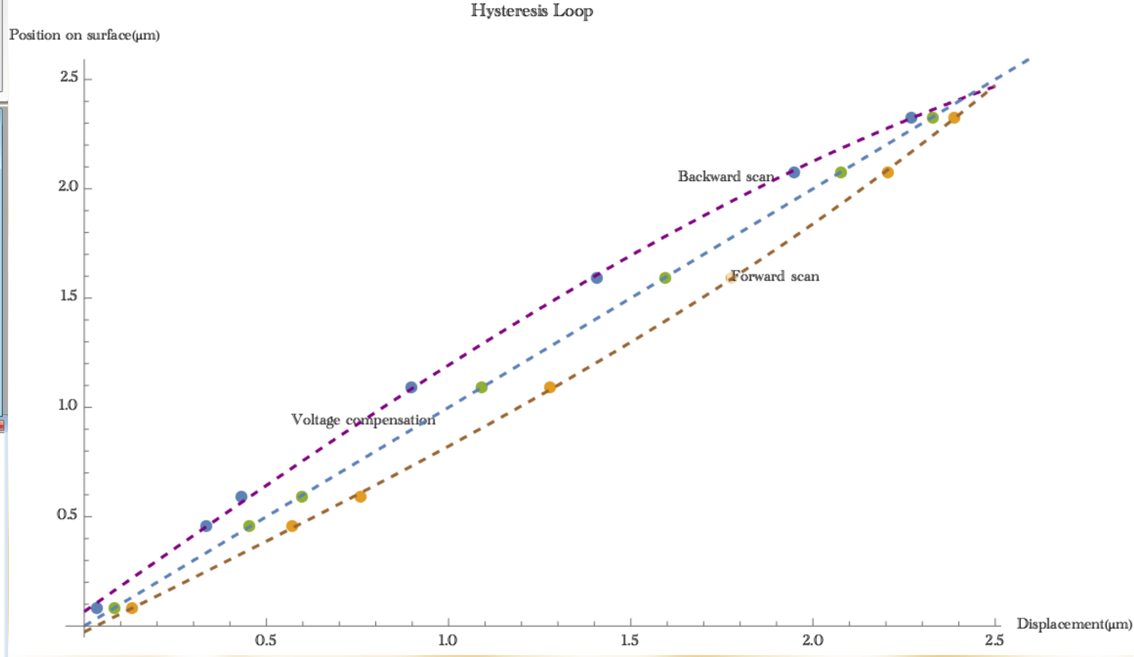

Electron Beam Ion Trap (EBIT)

- EBIS facility is a unique system, the only one in Poland and one of the few in the World, that allows the production of highly charged ions. Built by the Dreebit (Dresden, Germany), is equipped with electron beam ion trap (EBIS-A).
- The source supplies a wide range of slow highly charged ions from bare ions of light elements like Ne Ar to high-Z elements like Xe. The maximum electron energy and electron current available for ionization of the trapped ions are equal 25 keV and 200 mA, respectively.
- Typical ions: Ar^{18+} (fully ionized), Kr^{34+} (He-like), Xe^{44+} (Ne-like),

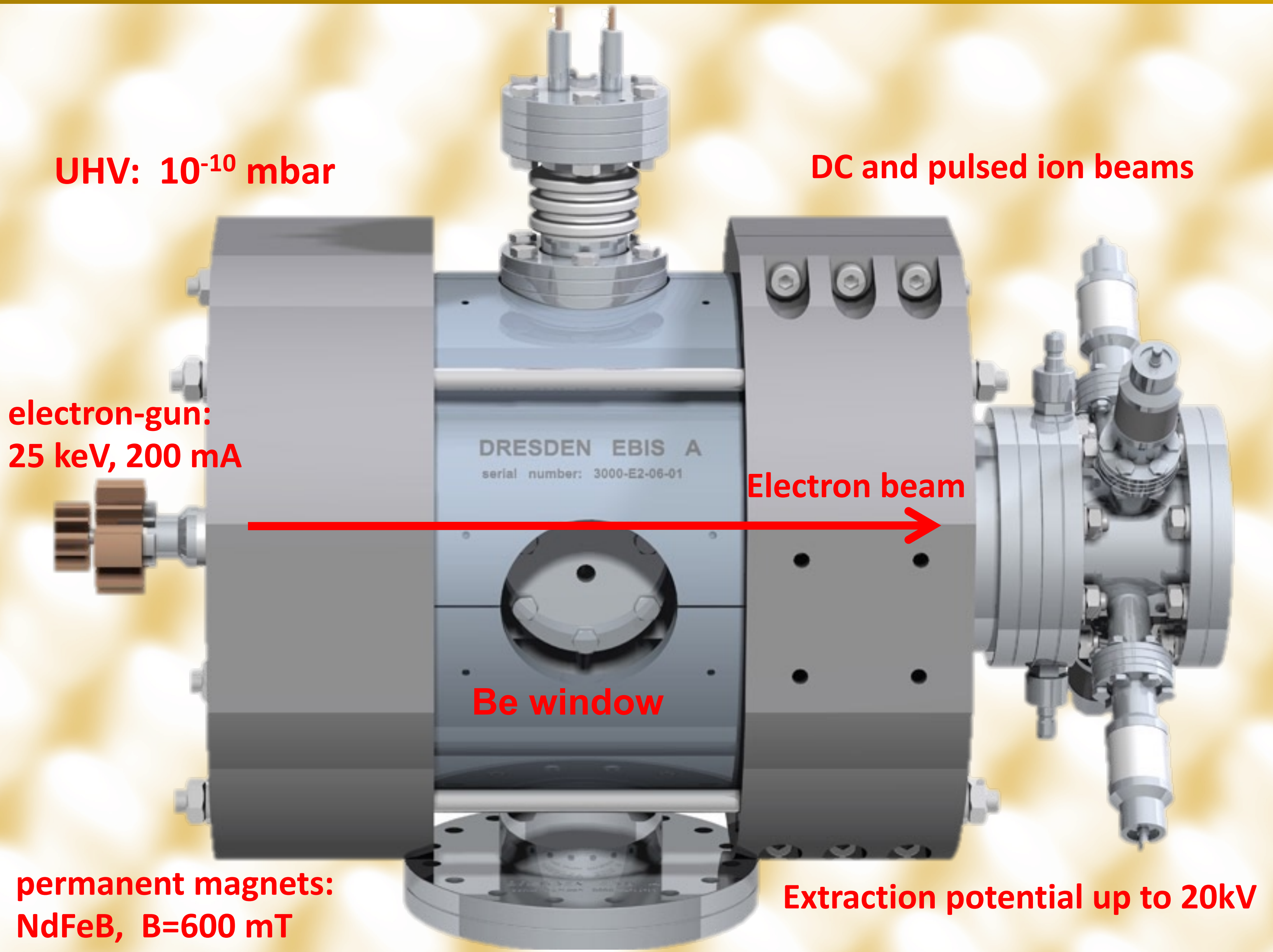

EBIS facility (Dreebit)

- Dresden EBIS-A ion source,
- beam guiding components,
- beam diagnostics,
- mass separation (double focusing analyzing magnet),
- multipurpose target chamber.

- ions energy from 20 eV x q to 40 keV x q
- ion acceleration and deceleration
- DC and pulsed beams (10ns to 100 μs per pulse)

DREEBIT Electron & Ion Beam Technologies

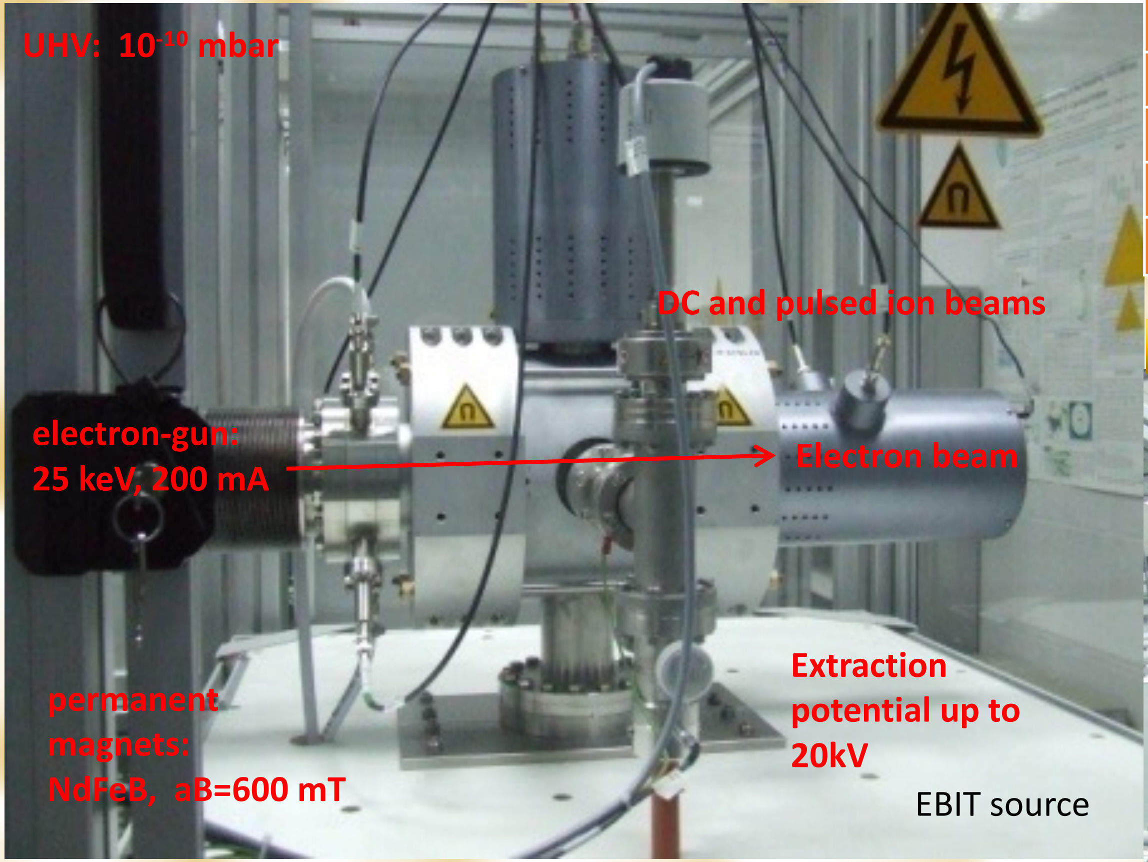

EBIT source

- EBIT trap length (6 cm), electron beam energy (25 keV) and current (200 mA), electron beam diameter (200μm), magnetic field strength (600 mT)
- typical ions: Ar^{18+}(fully ionized), Kr^{34+}(He-like), Xe^{44+}(Ne-like),

q	Ek[keV]	Ep[keV]	Ep/Ek
10	80	0,8	0,01
15	120	2,2	0,02
20	160	4,6	0,03
25	200	8,1	0,04
30	240	15,4	0,06
35	280	25,5	0,09
40	320	38,5	0,12
45	360	58,8	0,16
50	400	101,4	0,25

e.g. for 8kV Ek = q × 8keV:

HV supplies & controls

dipole magnet

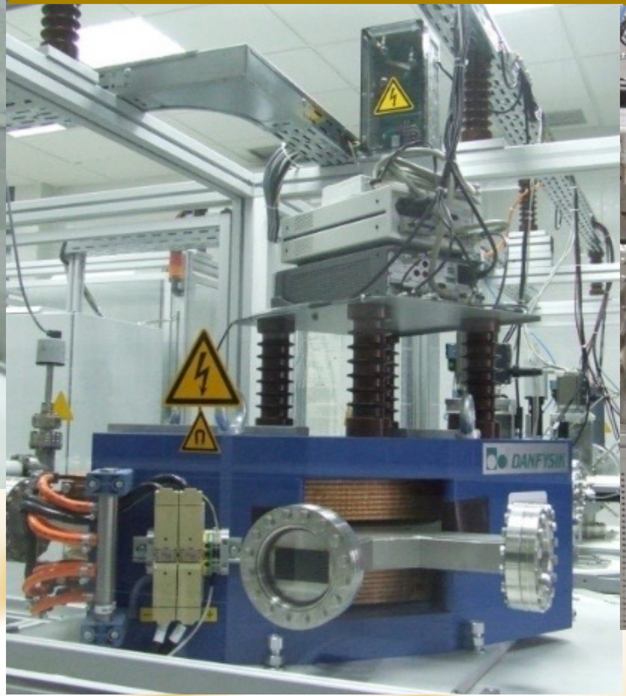

chamber (+XPS system)

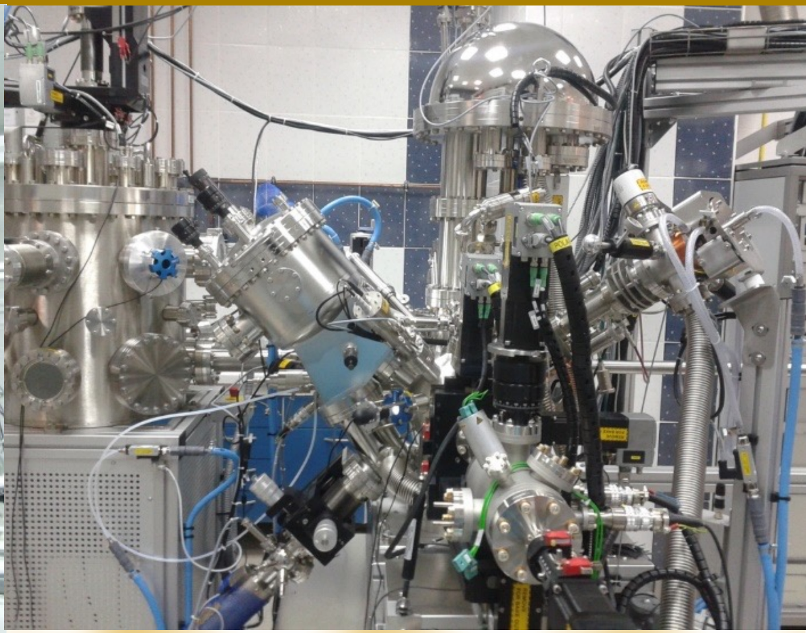

D. Banas et al., Nucl. Instr. Meth. B 354 (2015) 125

Highly charged ions (HCI)

Highly charged ion is any atom that has been stripped of a large number of electrons ($q \gg 1$).

A unique parameter for HCI is the **total potential energy E_{pot}**, which can be defined as the sum of the ionization energies E_j of all electrons removed from the atom:

$$E_{pot} = \sum_{j=0}^{q-1} E_{j\to j+1} \qquad E_{kin} = \frac{M_1 v_1^2}{2} = q \cdot U$$

where: M_1 – ion mass
v_1 - initial speed of the ion
q – charge state
U - acceleration voltage.

For example, a neutral Xe atom has 54 electrons (q = 54). The total potential energy E_{pot} of such ion (Xe^{54+}) is approximately 200 000 eV.

The term **slow highly charged ion** refers to ions which have a velocity v < 1 a.u.

- For slow ions, **nuclear stopping powers** dominate. These are elastic collisions of ions with the nuclei of the atoms of the target. The result is the delocalization of the atoms of the target and the creation of radiation defects.
- For high velocity v > 1 a.u. , **electronic stopping powers** dominate. These are inelastic collisions of ions with target electrons. The ion loses its energy in the process of excitation and ionization of the atoms of the target.

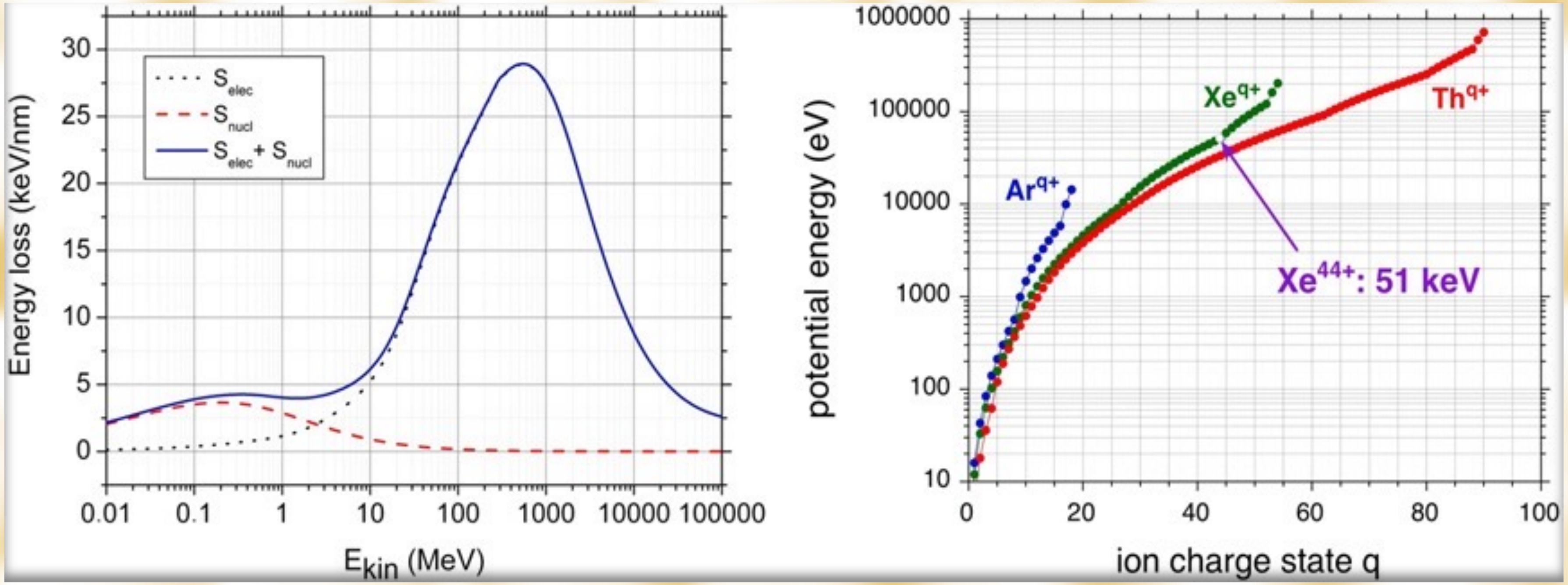

(a) Energy losses due to nuclear and electronic stopping as a function of kinetic energy in MeV as calculated with the SRIM code for the irradiation of SrTiO3 with Xe ions.
(b) Total potential energy of highly charged Ar^{q+}, Xe^{q+} and Th^{q+} ions versus charge state q. Xe^{44+}, for example, has a potential energy of about 51 keV.

Interaction of HCI ions with materials

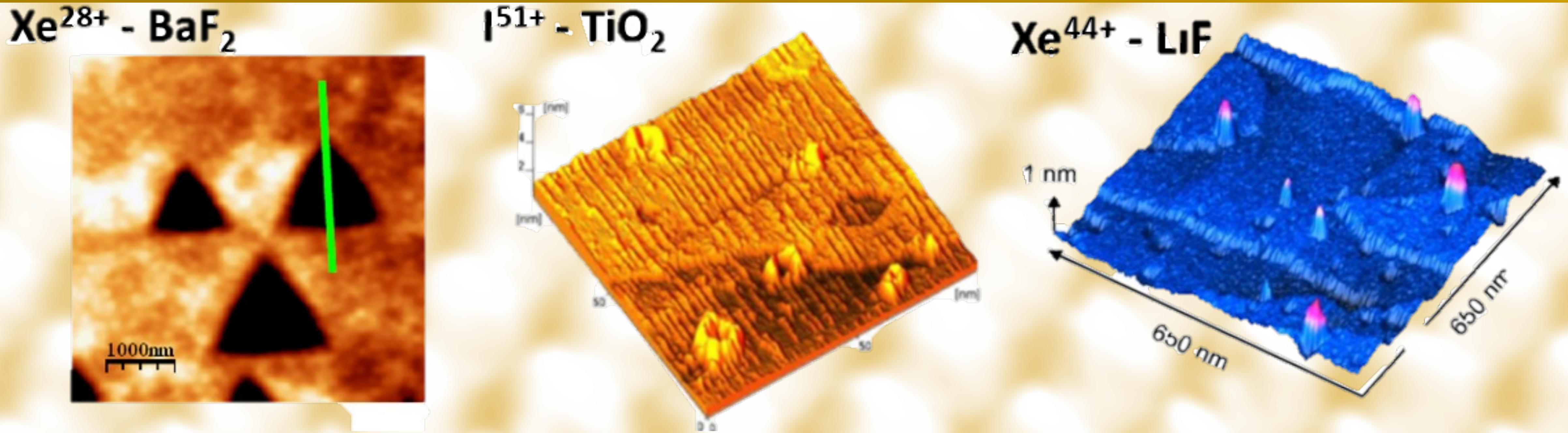

Figure: Nanostructures created using HCI can have a form of pits, hillocks or craters

- Most of the experimental observations were performed for insulators while for **semiconductors** (pure Si) and **metals** (Ti, Au) **only single experiments were carried out**.
- The reason for the small interest in this type of studies were the earlier experiments with swift highly charged ions, which suggested that in the interaction of such ions with materials of high thermal conductivity, the production of nanostructures is unlikely due to the rapid outflow of energy from the area of impact.

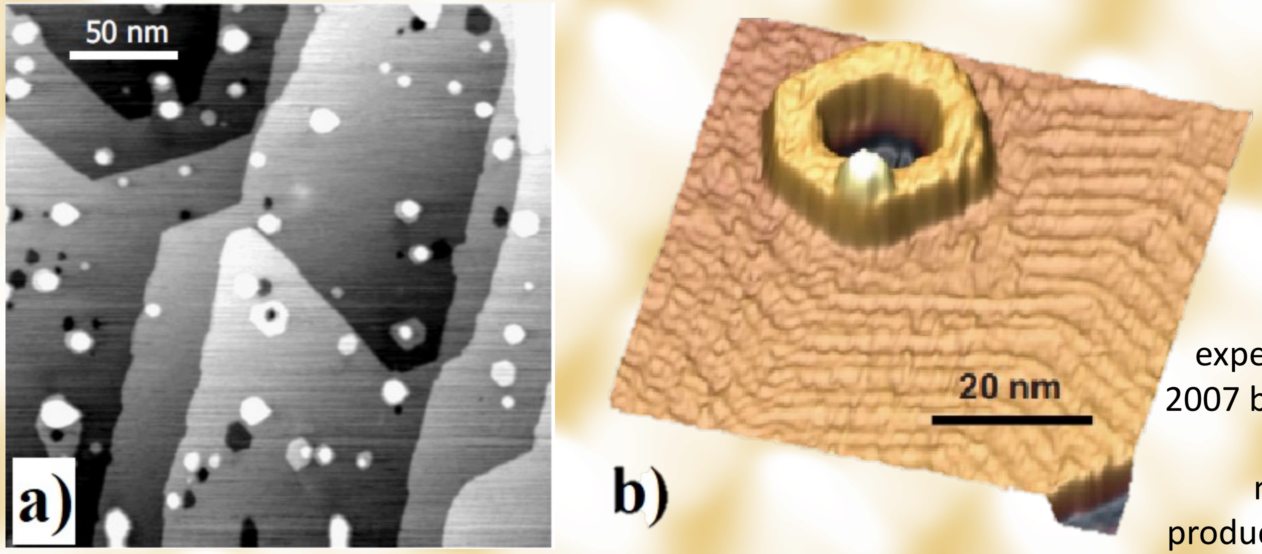

Figure: The results of experiments performed in 2007 by scientists from NIST in the USA. Different nanostructures can be produced by slow single HCI also on metallic surfaces.

HCI - solid surface interaction

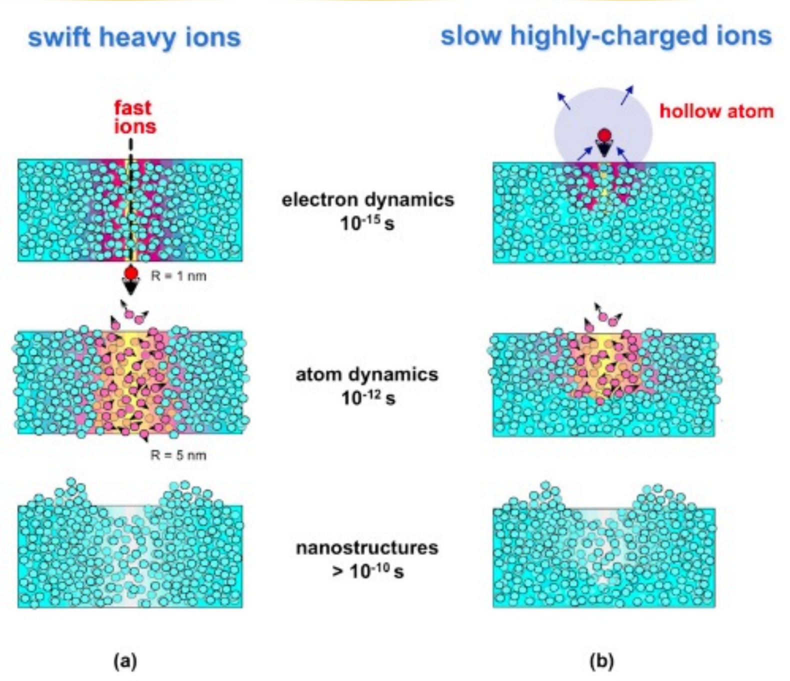

Time evolution of the interaction of (a) a swift heavy ion and (b) a slow highly charged ion with a solid surface. In both cases the initial interaction excites the electronic system on a femtosecond time scale, while atomic motion and creation of disorder happen on a picosecond time scale. Upon rapid thermal cooling, the disorder in the atomic system is quenched. On the surface, craters or hillocks of nanometric dimensions are formed. For SHI the damage extends deep into the bulk forming a cylindrical track: (a) has been reproduced with permission from.

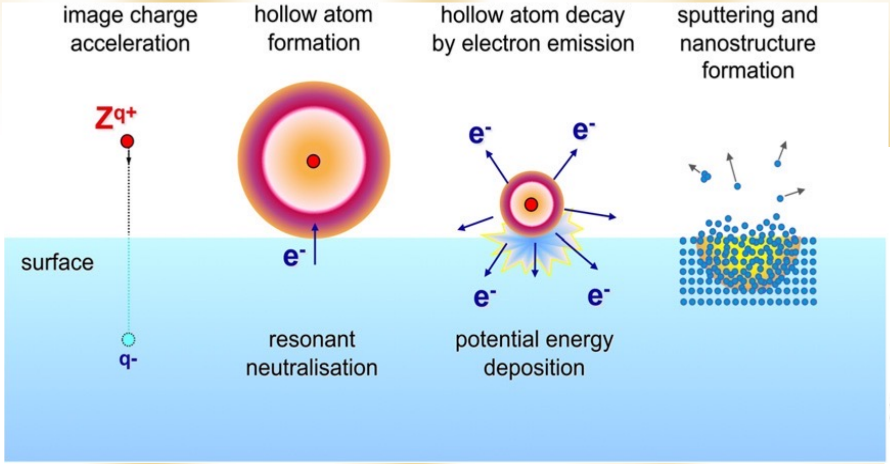

Current understanding of the interaction scenario when slow HCI impact a solid surface. From left to right: the HCI approaches the surface by acquiring image charge energy gain. Close to the surface, the ion picks up an electron from the target and forms a hollow atom. The hollow atom decays at and below the surface by electron- and x-ray emission. The potential energy of the HCI is deposited in a small volume close to the surface producing ionization and electronic excitation processes, eventually leading to potential sputtering and nanostructure formation.

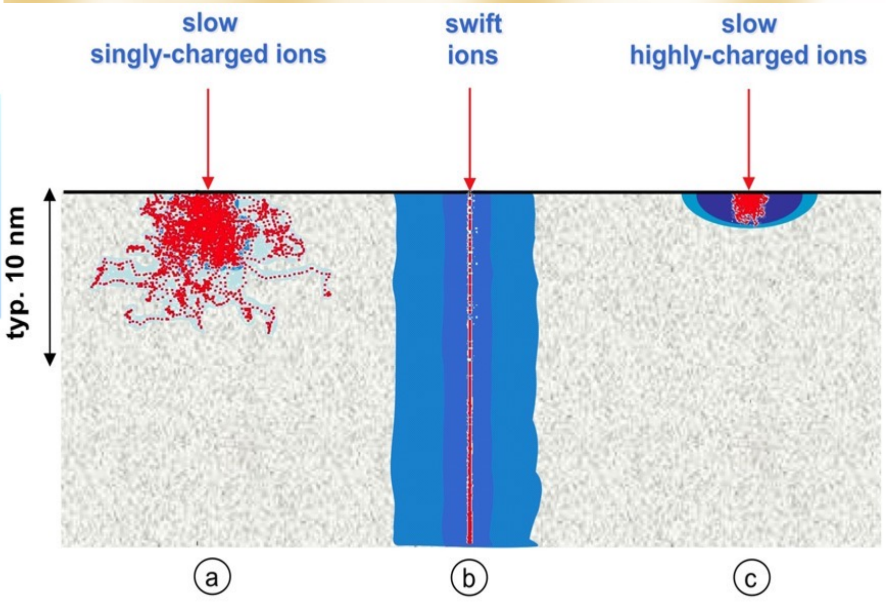

Scheme of energy deposition when ion projectiles interact with solids: (a) slow singly or low charged ions of keV–MeV kinetic energy: small range, energy loss dominated by elastic collisions (nuclear stopping), (b) swift ions of MeV–GeV kinetic energy, large range, energy loss dominated by electronic excitations, and (c) very slow highly charged ions, large potential energy (keV), very low (eV–keV) kinetic energy, very limited range. The trajectories of recoils are indicated in "red"; electron induced electronic excitations of the solid are marked in "blue".

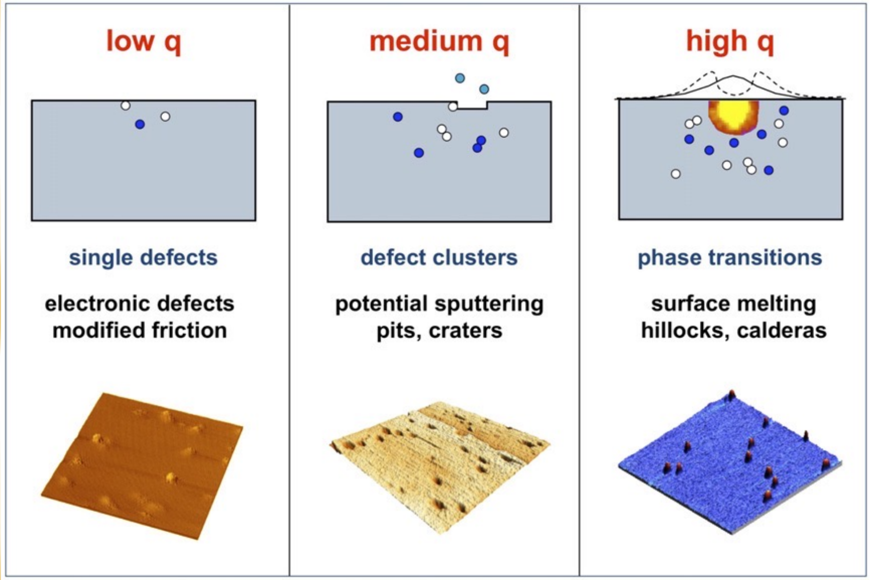

Scenario of defect creation for slow ions of different charge state *q*

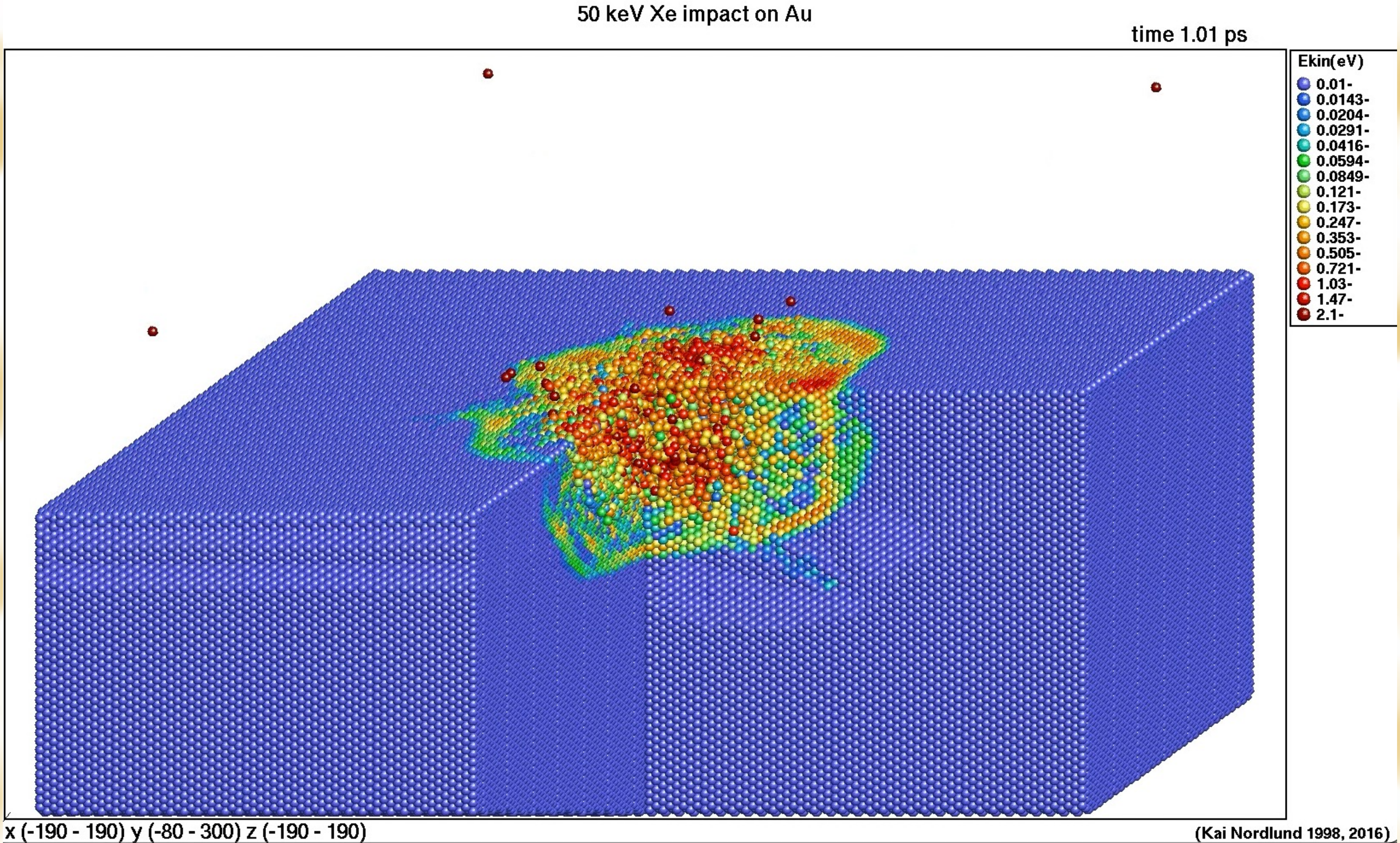
50 keV Xe impact on Au
time 1.01 ps
Ekin(eV)
0.01-
0.0143-
0.0204-
0.0291-
0.0416-
0.0594-
0.0849-
0.121-
0.173-
0.247-
0.353-
0.505-
0.721-
1.03-
1.47-
2.1-
x (-190 - 190) y (-80 - 300) z (-190 - 190)
(Kai Nordlund 1998, 2016)

Amorphous metals

Also known as **metallic glassess** were discovered in 1960 by Duwez during rapid soldification of small amounts of the alloy $Au_{75}Si_{25}$.
A great interest led to development numerous production methods during decades.
The most difficult in production of metallic glasses was that it required a cooling rate of at least the magnitude 10^5 K/s, what resulted in samples of thickness of the order of 1–100 mm.

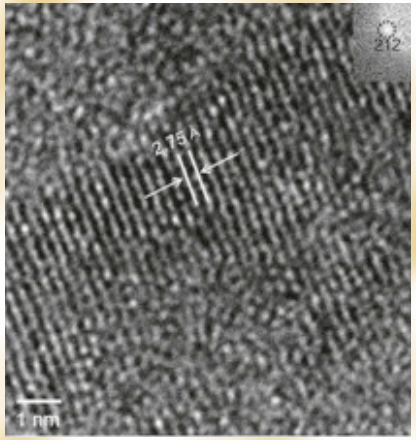

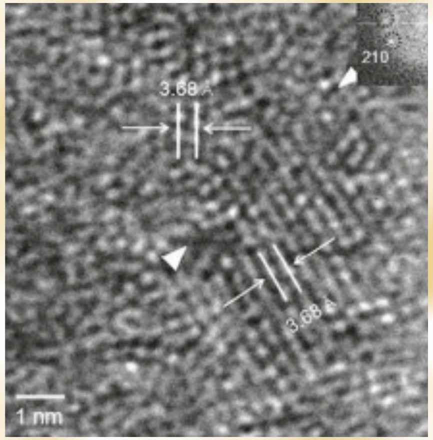

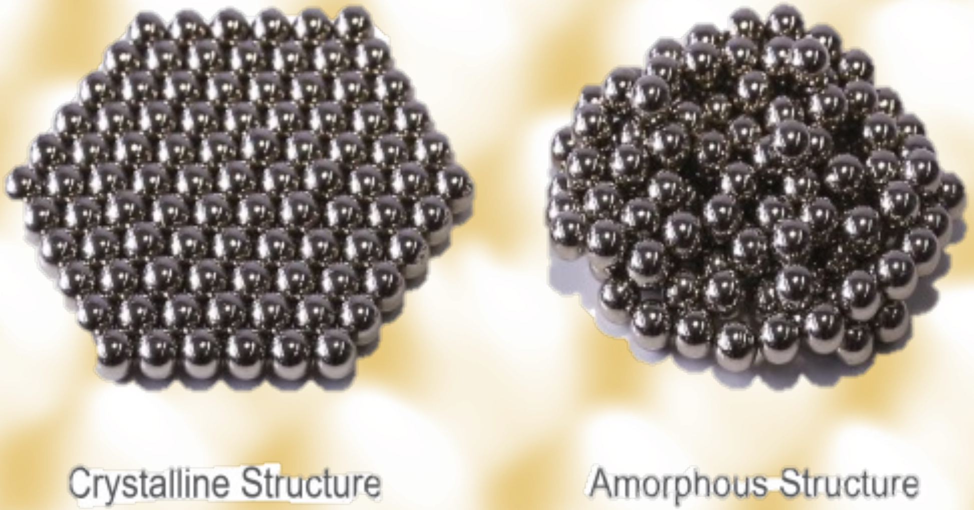

- Usually the alloys contains different size atoms that results in higher viscosity when melted
- No grain boundaries (defects) present in metals
- No shrinkage when cooled resulting in a resistance to plastic deformation
- Different properties that crystalline metals
- Need higher cooling rate than the characteristic to the alloy critical cooling rate

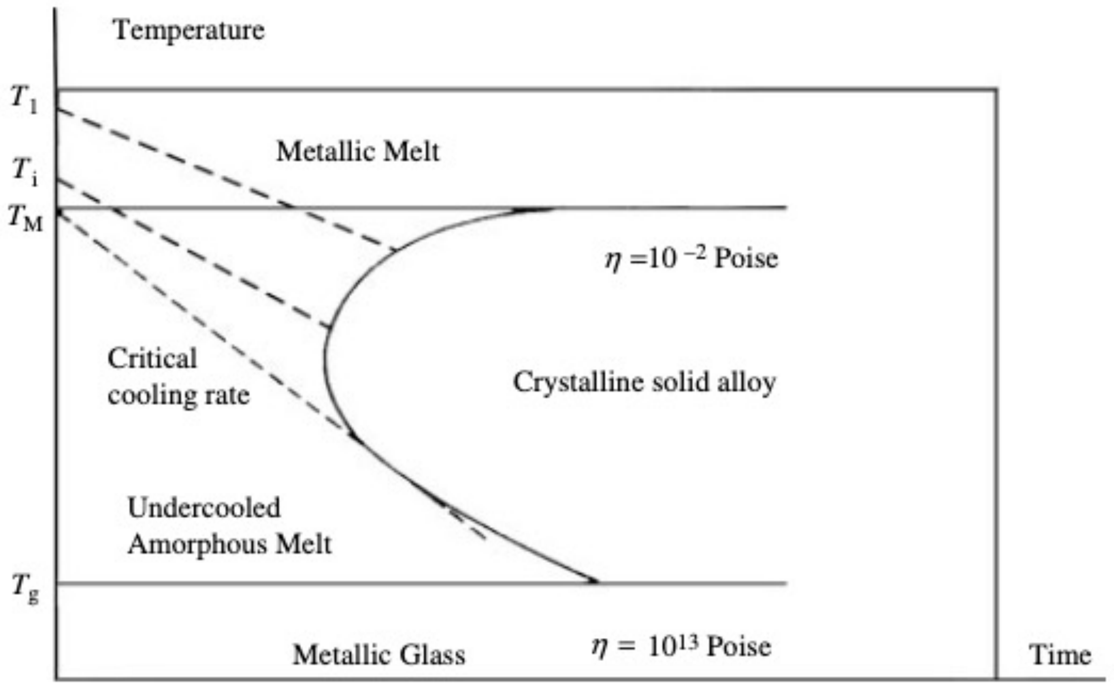

Continuous cooling transition diagram of an amorphous alloy

Measurements

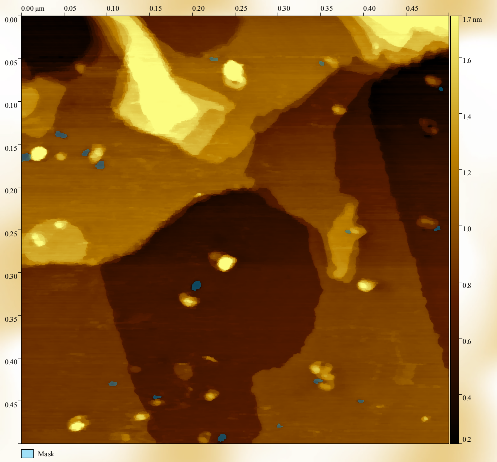

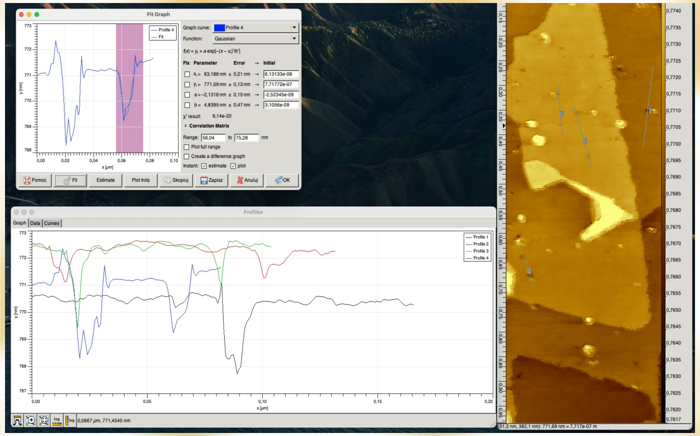

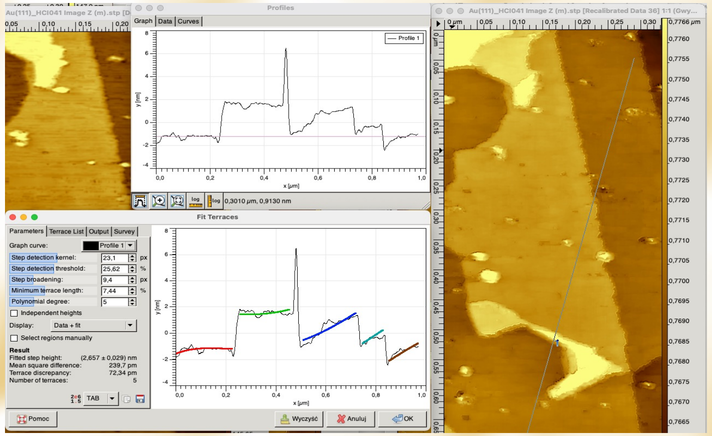

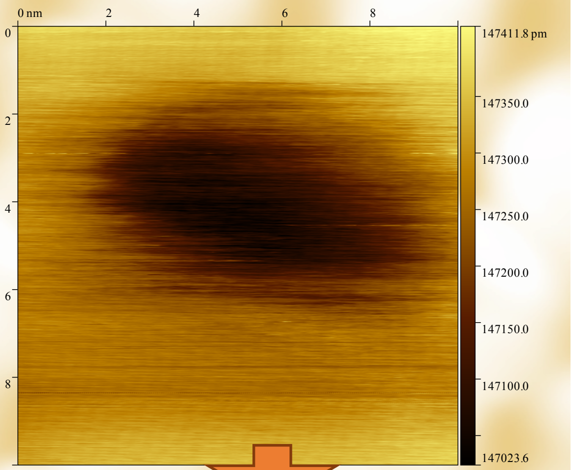

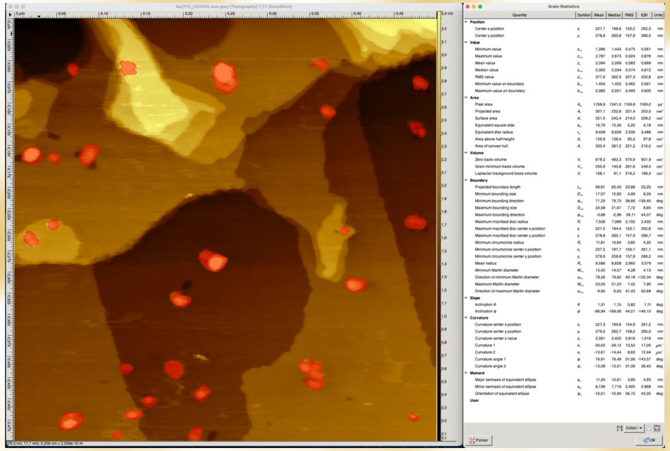

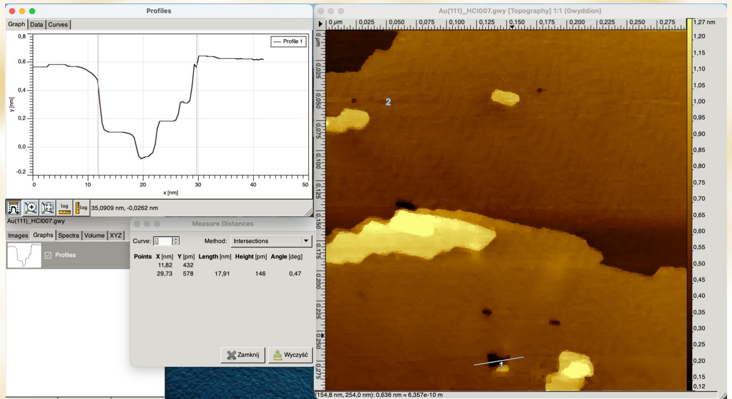

Roughness	HCI041		HCI042		HCI009		HCI007		HCI027		HCI040	
	no mask	mask	no mask	mask	no mask	mask	no mask	mask	no mask	mask	no mask	mask
RMS roughness (Sq) [pm]:	1292180	1290940	313,321	299,146	333,205	329,789	129,155	114,634	79,6195	15,8942	330,412	319,496
Minimum [nm]:	0	0	0,17132	0,17132	0	0	0	0	0	148,445	0	0
Maximum [nm]:	7,850	7,850	2,881	2,275	3,491	3,233	1,487	1,197	1,216	571,557	4,373	3,089
Median [nm]:	2,982	2,976	0,867	0,863	2,175	2,170	0,325	0,324	0,278	278,276	1,971	1,970
Maximum peak height (Sp) [nm]:	4,793	4,800	2,005	1,411	1,304	1,051	1,107	0,822	0,930	293,877	2,459	1,183
Maximum pit depth (Sv) [nm]:	3,057	3,049	0,705	0,693	2,186	2,181	0,380	0,375	0,286	129,235	1,913	1,906
Maximum height (Sz) [nm]:	7,850	7,850	2,710	2,104	3,491	3,233	1,487	1,197	1,216	423,112	4,373	3,089
Projected area [µm²]:	1	989106	250000	242291	250000	246819	90000	88359	20589	19777	250000	246783
Surface area [µm²]:	1	993088	250342	242520	250341	247118	90105	88456	20598	19781	250218	246973
ΔRMS	1240		14,175		3,416		14,521		63,7253		10,916	

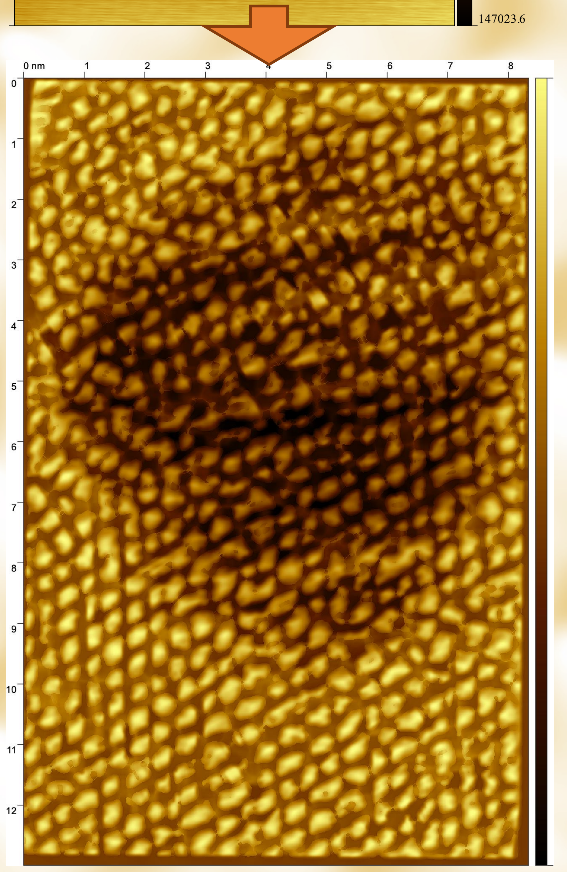

Measurements

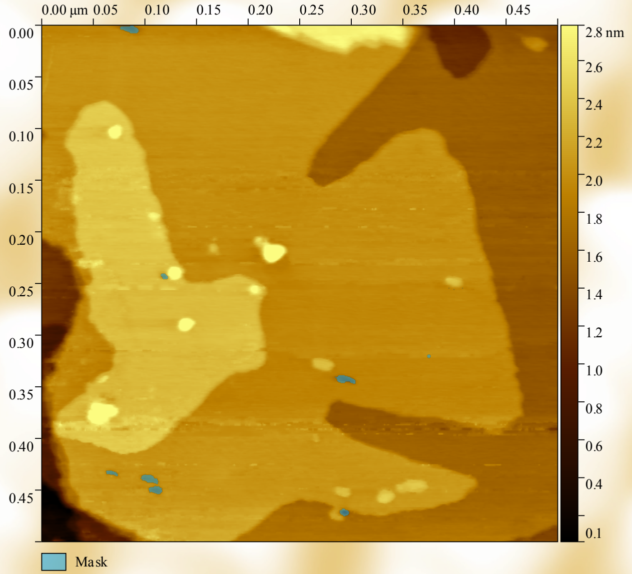

Holes 500x500 nm

	x	Height	Area of peak	Width	Height distance
	11,0	64,4	154615,0	0,7	155,4
	5,8	97,9	392035,0	1,3	156,5
	10,6	112,0	293714,0	0,9	116,3
	9,4	117,5	914797,0	2,1	275,4
	9,2	119,4	668616,0	2,4	133,7
	7,8	119,4	813039,0	2,9	134,8
	45,8	125,5	277077,0	0,9	210,1
	7,5	125,6	785945,0	2,5	204,3
	15,1	137,5	637002,0	1,4	187,0
	11,9	148,6	802194,0	2,0	165,9
	27,5	152,5	108862,0	2,2	101,4
	6,1	153,9	862646,0	1,8	166,3
	12,1	168,6	1453096,0	2,9	229,2
	26,1	175,0	1160649,0	2,3	244,9
	24,9	217,5	551449,0	2,0	243,5
	10,4	243,6	2006400,0	2,9	255,1
	4,5	265,9	1146138,0	1,5	309,8
	nm2	pm	pm2	nm	pm
Mean	14,7	155,0	804603,7	2,0	195,9
RMS	11,0	48,8	478082,2	0,7	60,6

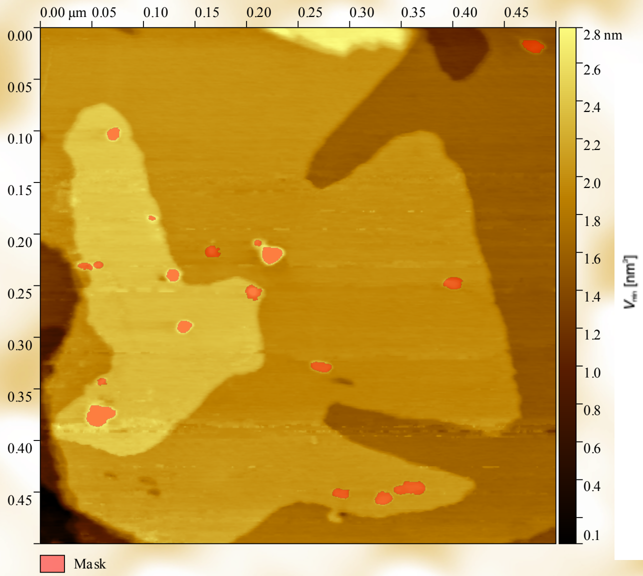

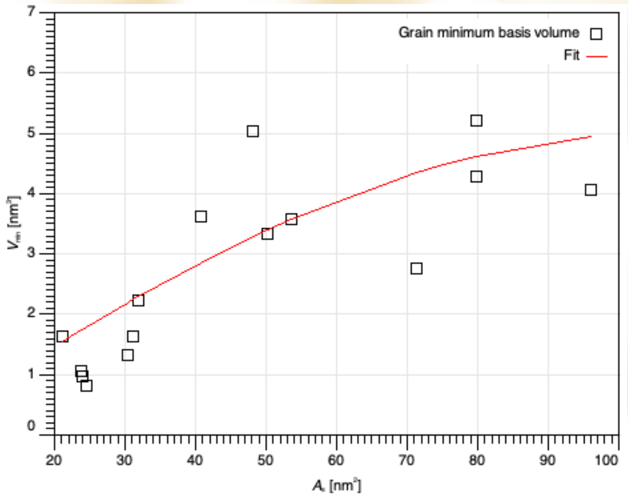

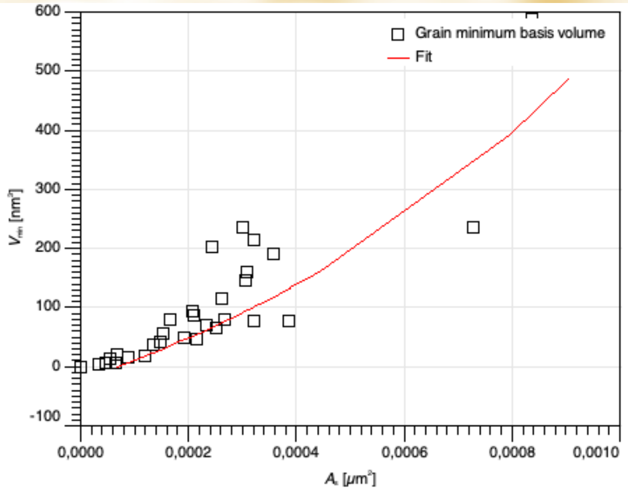

The dependence of the surface area of the holes and hillocks to the volume

Hills 500x500 nm

	x	Height	Area of peak	Width
	66,6	35,5	0,2	1,8
	71,8	74,6	1,3	0,8
	51,4	97,2	0,4	1,1
	33,2	109,8	0,3	1,0
	29,8	116,5	0,6	1,3
	60,8	127,7	0,8	1,9
	22,0	128,1	0,6	1,0
	49,2	144,1	1,2	2,0
	31,1	157,8	0,9	1,5
	76,1	164,7	1,5	2,6
	27,7	165,7	0,7	0,9
	27,6	180,1	1,5	1,9
	32,3	203,2	1,6	2,1
	28,8	238,2	2,8	3,4
	28,7	275,8	2,4	2,7
	27,7	283,9	3,0	3,5
	31,3	331,6	1,1	1,0
	28,4	339,7	2,5	1,9
	46,1	435,8	3,0	2,2
	31,0	446,1	3,6	3,0
	28,9	487,2	2,6	1,8
	30,5	502,6	4,6	2,3
	27,2	547,6	2,0	1,4
	29,4	598,5	6,8	2,6
	31,7	622,0	7,7	3,5
	30,2	659,4	7,2	3,7
	30,1	1148,3	10,4	3,2
	35,0	1305,2	21,1	5,6
	nm2	pm	nm2	nm
Mean	36,2	366,3	3,4	2,2
RMS	13,9	306,5	4,4	1,1

Measurements

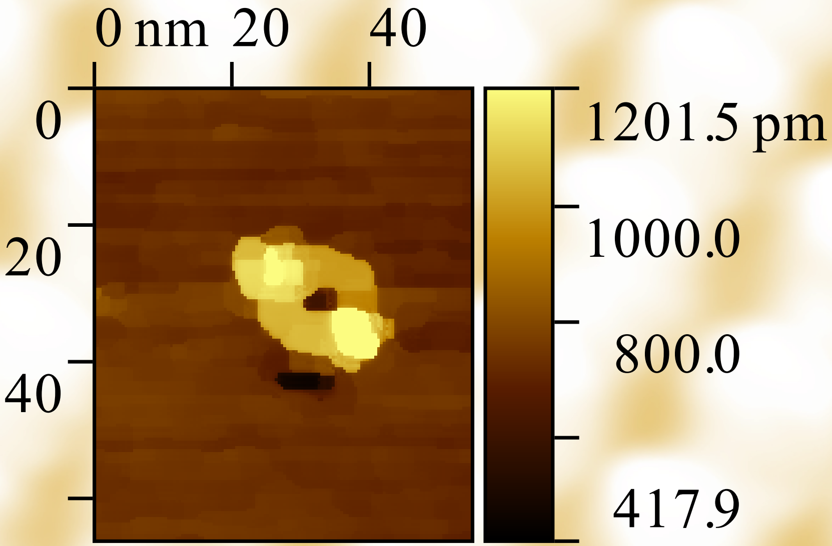

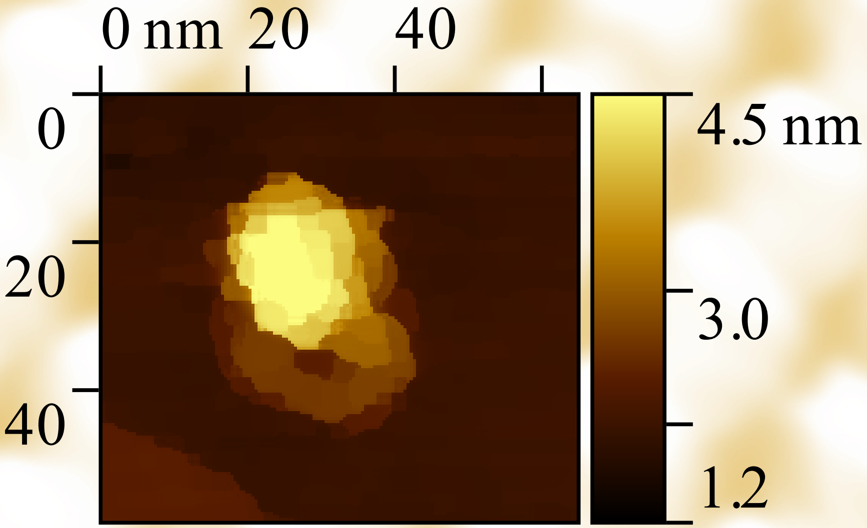

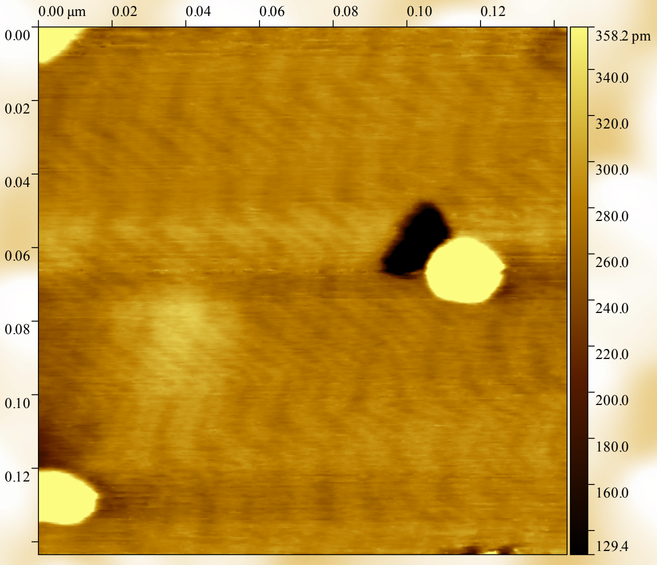

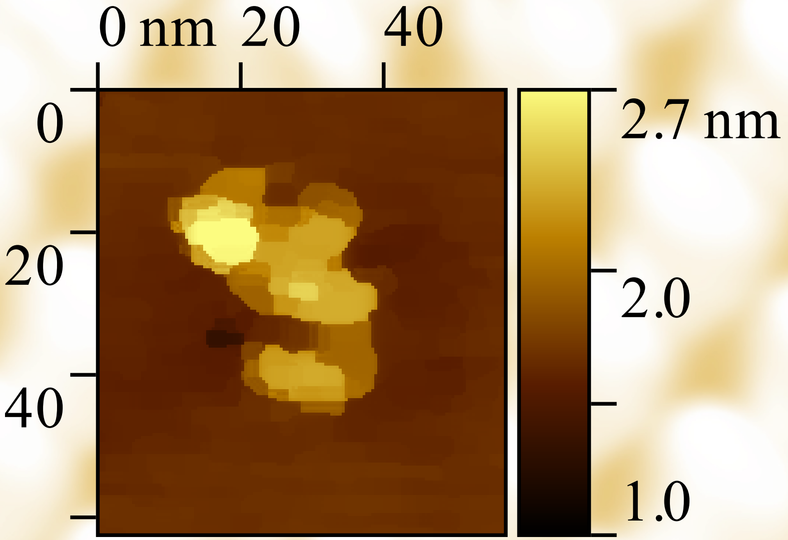

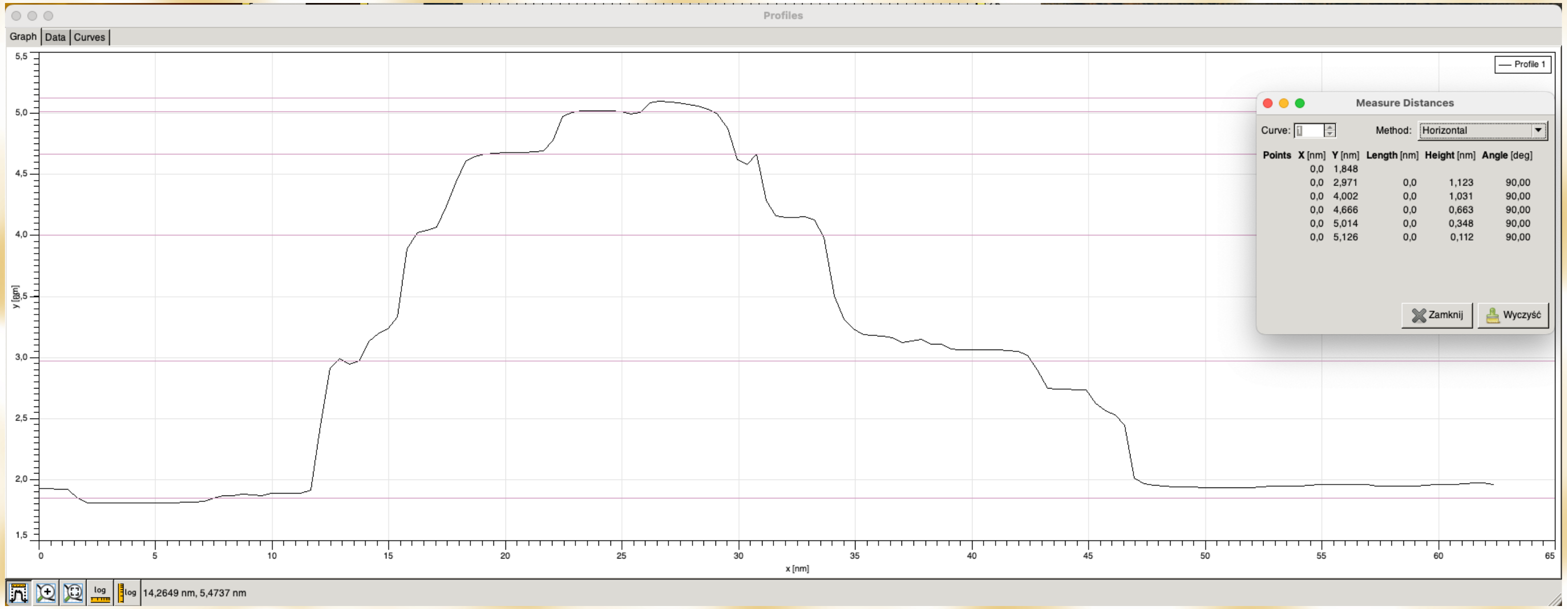

Thermal spike model

Within the analytical thermal spike (a-TS) model the various ion-induced physical effects are determined by the maximum temperature, and the actual time evolution of the temperature spike is not considered. It is assumed that the ion-induced temperature increase DT(r,t) can be approximated by a Gaussian distribution function, which is an analytical solution of

$$\Delta T(r,t) = \gamma S_e / \pi \rho c a^2(t) e^{-(r^2/a^2(t))}$$

$$\Delta T(R_m, 0) = T_0 = T_m - T_{ir}$$

$$R^2 = a^2(0)\ln(S_e/S_{et}) \text{ for } S_e < 2.7\, S_{et}$$

$$R^2 = (a^2(0)S_e)/(2.7S_{et}) \text{ for } S_e > 2.7\, S_{et}$$

$$S_{et} = (\pi \rho c T_0 a^2(0))/\gamma$$

$$\gamma = 2.7\pi \rho c T_0 R^2 / S_e.$$

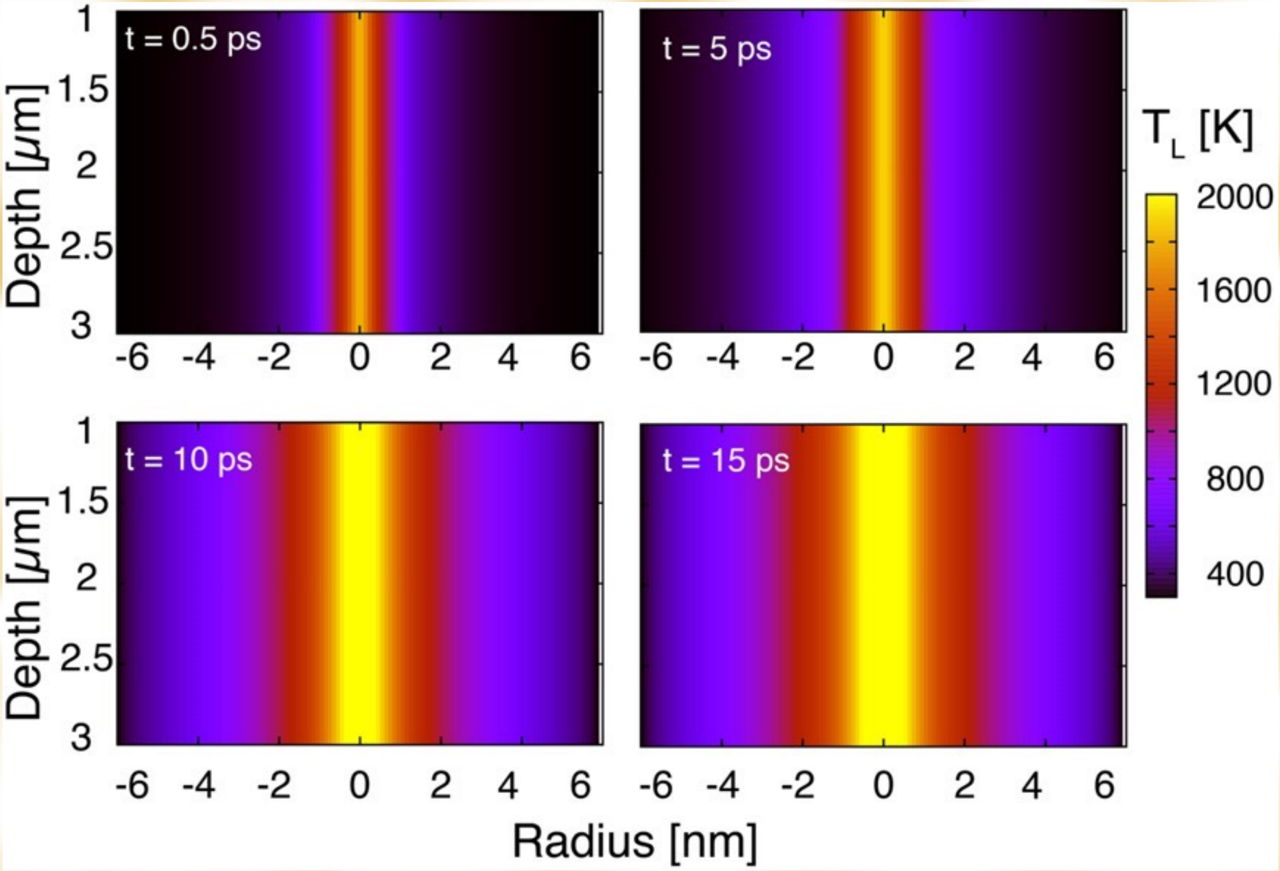

Thermal spike model

Summary		HCI006	HCI040	HCI042	HCI041	HCI007	HCI009	HCI027		
No. of grains		7	18	34	88	7	30	3	Mean	RMS
Mean radious of hillock		5,648	6,754	7,256	5,439	6,666	4,916	7,042	6,25	0,90
Max martin diameter		13,89	16,63	11,32	14,52	18,93	14,55	16,04	15,13	2,39
Single hillock mean volume	nm3	12,37	43,9	59,69	37,27	21,52	16,4	48,14	34,18	17,80
Mass of the atoms at the initial volume	g	2,04E-19	6,25E-19	9,68E-19	6,12E-19	2,87E-19	2,77E-19	6,84E-19	5,22E-19	2,77E-19
Mass of the atoms at the initial volume in atomic units	u	122560,67	376621,79	583124,86	368539,03	172760,40	166637,16	411775,06	314574,14	166930,77
No. of atoms with the mass equivalent to the initial volume		622	1912	2960	1871	877	846	2091	1597	847
The total mass of the atoms at the hillock volume	g	2,1412E-19	7,5991E-19	1,0332E-18	6,4514E-19	3,7251E-19	2,8388E-19	8,333E-19	5,92E-19	3,08E-19
The total mass of the atoms at the hillock volume in atomic units	u	128948,82	457627,58	622227,57	388514,35	224331,34	170958,82	501826,69	356347,88	185587,43
No. of atoms with the mass equivalent to the hillock volume		655	2323	3159	1972	1139	868	2548	1809	942
No. of atoms equivalent to the mean initial volume		624	1917	2968	1876	879	848	2096	1601,29	849,74
The volume equivalent to a single atom, suitable to the calculated initial conditions	nm3	0,0169	0,0170	0,0169	0,0169	0,0168	0,0170	0,0169		
The radius equivalent to a single atom, suitable to the calculated initial conditions	nm	0,159	0,159	0,159	0,159	0,159	0,159	0,159		
The volume equivalent to a single atom, suitable to the hillock volume	nm3	0,020	0,023	0,020	0,020	0,025	0,019	0,023	0,02	0,00
The radius equivalent to a single atom, suitable to the hillock volume	nm	0,168	0,176	0,169	0,168	0,180	0,167	0,176	0,17	0,01
dV	nm3	1,830	11,470	9,520	5,560	6,760	2,060	12,710	7,13	4,32
dV	%	17,36	35,37	18,98	17,53	45,80	14,37	35,87	26,47	12,29
dT	K	4133,91	8421,07	4517,97	4174,74	10904,63	3420,34	8541,32	6302,00	2926,94
free volume	atoms	32	411	199	101	262	22	457	212	175
Thermal spike model dT[r]	K	4120,88	8447,01	4517,35	4176,07	10661,7	3425,68	8542,74	6270,20	2868,13
Thermal spike model - initial volume	nm3	10,54	32,40	50,17	31,71	14,86	14,34	35,43	27,07	14,36
Temperature increase in the eV units	eV	0,355	0,728	0,389	0,360	0,919	0,295	0,736	0,54	0,25
Energy/atom	eV/atom	28,39	58,20	31,12	28,77	73,46	23,60	58,86	43,20	19,76
Energy in the atomic units	a.u.	0,01	0,03	0,01	0,01	0,03	0,01	0,03	0,02	0,01

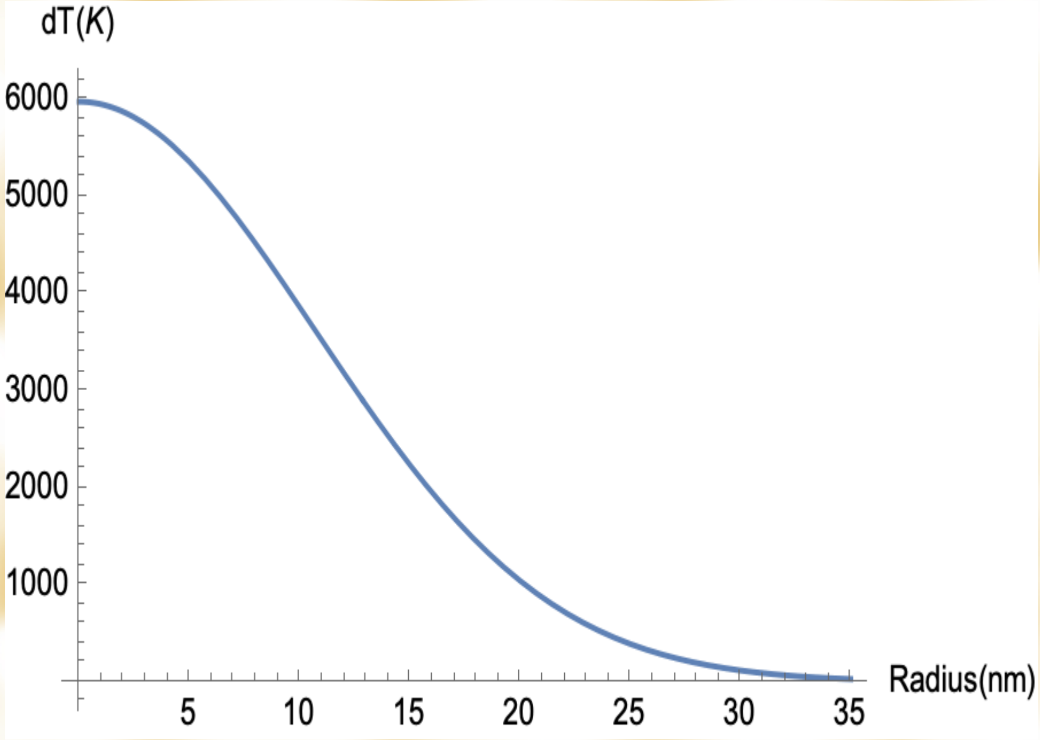

Radial temperature distribution of the mean of experimental points

Conclusions

- Modifications of gold nanolayers in collision with individual Xe HCI were studied in the ion's energy range hundreds of keV
- The measurements demonstrate that the nanostructures can be efficiently created with Xe HCI also on metallic surfaces
- The measurements show that potential energy of HCI has sufficient magnitude to melt the gold surface
- Atomic viscosity and relaxation time is needed to determine the type of the structure of the modified regions

In the near future

- Cooperation with IMIF (Instytut Mikroelektroniki i Fotoniki) Łukasiewicz
- Measurements and characterization of new metallic nanolayers:
  a) Iridium
  b) Platinum
  c) Palladium (received)
  d) Copper
  e) Titanium (received)
- Validation check of the effective time of physical vapor deposition (PVD) in getting continuous nanolayer structure
- Perform a measurements of nanolayers irradiated with HCI
- Checking the measurements theory
- Start up AFM measurements
- Molecular dynamics modelling